Extra-galactic and survey science with the Submillimeter Common User Bolometer Array-2

by

Todd Mackenzie

B.Sc., The University of Prince Edward Island, 2009

A THESIS SUBMITTED IN PARTIAL FULFILLMENT OF
THE REQUIREMENTS FOR THE DEGREE OF

MASTER OF SCIENCE

in

The Faculty of Graduate Studies

(Astronomy)

THE UNIVERSITY OF BRITISH COLUMBIA

(Vancouver)

October 2011

Abstract

We have carried out a pilot study for the SCUBA-2 'All-Sky' Survey, SASSy, a wide and shallow mapping project at 850 μm, designed to find rare objects, both Galactic and extragalactic. Two distinct sets of exploratory observations were undertaken, and used to test the SASSy approach and data reduction pipeline. The first was a $0.5^\circ \times 0.5^\circ$ map around the nearby galaxy NGC 2559. The galaxy was easily detected at 156 mJy, but no other convincing sources are present in the map. Comparison with other galaxies with similar wavelength coverage indicates that NGC 2559 has relatively warm dust. The second observations cover 1 deg^2 around the W5-E H II region. As well as diffuse structure in the map, a filtering approach was able to extract 27 compact sources with signal-to-noise greater than 6. By matching with data at other wavelengths we can see that the SCUBA-2 data can be used to discriminate the colder cores. Together these observations show that the SASSy project will be able to meet its original goals of detecting new bright sources which will be ideal for follow-up observations with other facilities.

We have also carried out a study of MS 0451−03, a massive galaxy cluster at z=0.5, strongly lensing a group of galaxies at z=3. Imaging with SCUBA, and more recently with SCUBA-2, shows a prominent arc of submm emission, but lacks the resolution to break up this lensed structure into individual sources. ALMA, even in Early Science mode, has the ability to finally resolve the giant submm arc. A lensing reconstruction will allow us to relate the submm sources to lensed objects detected in other wavebands. The cluster-scale lensing and the extent of the galaxy group make this a relatively simple system to investigate. Lessons learned here could help us understand the effects of differential lensing on the spectral energy distribution in more complicated galaxy-scale lens systems.

Preface

- Chapter 2 has been published as a paper in Monthly Notices of the Royal Astronomical Society [MacKenzie et al., 2011] and has been co-authored with Douglas Scott, Filiberto Braglia, Andy Gibb and others, with myself as the primary author. Since this was the first paper from a long-planned survey (The SCUBA-2 All Sky Survey), the author list contains all the researchers who were actively involved in the survey planning. For the sections on fitting modified blackbody spectral energy distributions, some of the initial work and was performed by Filiberto Braglia.

Table of Contents

Appendices

List of Tables

List of Figures

Acknowledgements

First, I would like to thank my supervisor, Dr. Douglas Scott. He has both guided me through my research and all the hurdles one must go through to complete a Masters degree. Along with his guidance, he has also given me much independence and allowed me a much appreciated flexible schedule.

Second, I would like to thank my colleagues, Andy Gibb, Filiberto Braglia and Edward Chapin, who helped me through technical problems, helped perform the research we have undertaken, and with whom I have collaborated with writing my published paper [MacKenzie et al., 2011]. Without them, much of this work would not have been completed.

I must thank the sources of the funding I have received: my supervisor and NSERC for my salary and conference support, the department of physics and astronomy for tuition support and top-up bursaries, NSERC through an Alexander Graham Bell Canada Graduate Scholarship during my first year, UBC for a graduate fellowship during my second year, and the Joint Astronomy Centre in Hawaii for my journey to finally meet "my telescope".

Finally, I must thank my parents for the support and freedom they have given me through all my studies.

Below are acknowledgments to the telescope facilities and organizations which this research has relied upon.

The James Clerk Maxwell Telescope is operated by The Joint Astronomy Centre on behalf of the Science and Technology Facilities Council of the United Kingdom, the Netherlands Organisation for Scientific Research, and the National Research Council of Canada. Data for this paper were taken as part of the S2SRO programme, with Project ID M09BI142.

This research used the facilities of the Canadian Astronomy Data Centre operated by the National Research Council of Canada with the support of the Canadian Space Agency.

This research was supported by the Canadian Natural Sciences and Engineering Research Council and enabled through funding from the Canada Foundation for Innovation and through the CANFAR Programme, funded by CANARIE, Canada's advanced Internet organization.

This work is based in part on observations made with the *Spitzer Space*

Telescope, which is operated by the Jet Propulsion Laboratory, California Institute of Technology, under a contract with NASA.

This research is based in part on observations with *Akari*, a JAXA project with the participation of ESA.

This research has made use of the NASA/IPAC Extragalactic Database (NED) which is operated by the Jet Propulsion Laboratory, California Institute of Technology, under contract with NASA.

The Digitized Sky Surveys were produced at the Space Telescope Science Institute under U.S. Government grant NAG W-2166. The images of these surveys are based on photographic data obtained using the Oschin Schmidt Telescope on Palomar Mountain and the UK Schmidt Telescope.

The VLA is part of the US National Radio Astronomy Observatory, a facility of the National Science Foundation operated under cooperative agreement by Associated Universities, Inc.

Chapter 1

Introduction to SCUBA-2

1.1 Introduction to the JCMT and the new SCUBA-2 instrument

The Submillimeter Common User Bolometer Array-2 (SCUBA-2) is a submillimeter instrument aboard the James Clerk Maxwell Telescope (JCMT) in Hawaii. The JCMT is currently the largest operational single-dish submm telescope in the world and has been ranked as one of the highest impact telescopes ever since SCUBA was installed, falling second only to the Hubble Space Telescope [Davis et al., 2010]. SCUBA was decommissioned in 2005 with SCUBA-2 as its replacement with the goal of greatly improving mapping speed and sensitivity in the sub-mm spectrum. With the new improved sensitivity and a larger field of view (FOV), SCUBA-2 will be ideal for peforming large sky surveys.

1.2 SCUBA vs. SCUBA-2

The original SCUBA instrument operated on the telescope for 7 years. It consisted of 37 and 91 bolometers at 450 and 850 μm respectively, arranged in a hexagonal pattern, and read-out at a rate of 1 Hz. Over its lifespan, SCUBA was able to map approximately 29 deg^2 of the night sky to varying depths [Di Francesco et al., 2008]. SCUBA-2 has four arrays at each wavelength. Each array has 32×40 bolometers, each with a read-out rate of 200Hz, and together they cover a larger FOV than SCUBA. Comparing bolometer to bolometer, SCUBA-2 bolometers are more sensitive than those found in SCUBA. Initial estimates suggested SCUBA-2 to be over a thousand times as fast SCUBA for mapping the sky.

For SCUBA-2, the bolometers employed are transition edge sensor (TES) bolometers paired with Superconducting QUantum Interference Devices (SQUIDs). Bolometers are detectors that rely on temperature changes induced by incident photons. TES bolometers use a thin film that operates within the temperature region where the material transitions from being

superconducting to normally conducting [Irwin and Hilton, 2005]. Within this region, the resistance of the material is very sensitive to temperature changes, making it ideal for detecting small changes in temperature, and therefore ideal for detecting submillimeter photons. When a photon is incident on the TES bolometer, the rise in temperature changes its resistance and therefore changes the current running through the TES. The resistance produced by the TES is of order milli-ohms, therefore the current fluctuations are very small. In order to detect such small current fluctuations, the signal is amplified using DC SQUID amplifiers.

DC SQUIDs are used to detect very small changes in magnetic field [Clarke and Braginski, 2004]. By running the TES current through a coil, a magnetic field can be generated that is coupled to the SQUID. Each SQUID consists of a superconducting ring with two Josephson junctions and is able to detect very small magnetic field fluctuations caused by the TES current and is read-out by the SCUBA-2 electronics.

Both the TES bolometers and the DC SQUIDs require SCUBA-2 to be at very low temperatures. SCUBA-2 has several layers of cooling arranged in shells: a 60 K shell, a 4 K shell, a 1 K shell, and finally the arrays operate at below 100 mK. The instrument is initially cooled with liquid nitrogen, but remains cool without any need for more liquid cryogens. Instead, Cryomech pulse tube coolers are used for cooling the outer parts of the instrument. A Leiden Cryogenics dilution refrigerator, pulse tube cooler and Joule-Thomson Heat exchanger cools the 1 K section and the mixing chamber cool the focal planes to below 100mK.

The whole instruments weighs approximately 4 tonnes and is mounted onto the nasmyth focus of the JCMT. To accommodate such a large instrument, structural modifications to the telescope were necessary and the focal plane was required to be re-imaged to the size of the arrays (from approximately 66 to 10 cm)[Holland et al., 2006].

1.3 SCUBA-2 commissioning status

Although not fully comissioned, there was a period of a few months of shared risk observing (SRO) at the beginning of 2010. During this time, the JCMT Legacy Survey groups were given SCUBA-2 observing time using one of four detector arrays at each wavelength (the others were not yet installed). This allowed the survey teams to familiarise themselves with the observing tools, SCUBA-2 data and analysis software, and to reassess their survey capabilities. It was during this time that the observations used in the next

sections were taken. New estimates of mapping speed put SCUBA-2 at a few hundred times that of SCUBA.

Chapter 2

A pilot study for the SCUBA-2 'all-sky' survey

2.1 Introduction

The millimetre and sub-millimetre parts of the electromagnetic spectrum directly probe the cold Universe. The sub-mm window specifically allows us to study the youngest phases of star formation in our Galaxy, and the dusty, most prodigiously star-forming galaxies at high redshift. Despite this strong motivation, the sub-mm sky still remains poorly surveyed. The SCUBA-2 'All-Sky' Survey, or SASSy[1], is a JCMT Legacy Survey (JLS) project designed to redress this balance and exploit the rapid mapping capability of SCUBA-2 to ultimately map a large portion of the sky visible from the JCMT to an angular resolution of 14 arcsec at 850 μm. The target point source rms level is 30 mJy.

The benefits of such a wide-field survey are many, ranging from a complete census of infrared dark clouds (IRDCs) to the potential discovery of some of the most luminous high-redshift galaxies in the Universe [Thompson et al., 2007]. The approved phase of SASSy consists of two distinct parts: a strip covering the Galactic Plane which is visible from Hawaii; and a 'Pole-to-Pole' strip perpendicular to this and designed to pass through the Galactic and Ecliptic North Poles. These observations will be carried out in 'Grade 4' weather conditions ($0.12 < \tau_{225} < 0.2$, where τ_{225} is the sky opacity at 225 GHz, as measured by the CSO radiometer), i.e. essentially when the atmosphere is too opaque to enable useful observations of fainter objects with SCUBA-2. The 450 μm data are therefore expected to be of marginal value, and the survey is entirely designed to make large maps at 850 μm, with a target sensitivity of 30 mJy, achieved using a fast scanning speed.

SASSy will be able to build on the success of *IRAS* at one decade shorter wavelengths. It is also complementary to several more recent wide surveys,

[1] Alternatively known as the SCUBA-2 Ambitious Sky Survey.

namely *WISE* and *Akari*, at near- and mid-IR wavelengths, and surveys with the *Herschel* and *Planck* satellites in the submillimetre (hereafter submm). Early results from *Herschel* have already demonstrated that bright lensed galaxies can be selected at submm wavelengths [Negrello et al., 2010a], and also that potentially protostellar cores can also be found using *Herschel* [Ward-Thompson et al., 2010]. The *Planck* Early Release Compact Source Catalogue will contain an all-sky list of sources which includes the 850 μm channel. However, the resolution of SASSy will be 20 times better. Hence it is clear that if SCUBA-2 is able to map rapidly enough while maintaining its nominal beam-size and achieving the required sensitivity, then SASSy will be able to meet its science goals. As we show below, these preliminary SCUBA-2 data lend confidence that these requirements can be met and that SASSy will discover many new and interesting sources.

In the next section we describe the two sets of observations which were made as a pilot study for SASSy, one Galactic field and one extragalactic field. In Section 2.3 we describe how we reduced the data and extracted sources. We then discuss the properties of the sources that we found and end with some conclusions about SASSy in general.

2.2 Observations

SCUBA-2 [Holland et al., 2003, 2006] is the successor to the Submillimetre Common User Bolometer Array (SCUBA, Holland et al. 1999), which operated successfully on the JCMT from 1997–2005. SCUBA-2 has been designed to be hundreds of time faster than SCUBA for mapping the sky in the same two primary bands, 450 μm and 850 μm. The observatory offered a period of 'Shared Risks Observing' programme (hereafter S2SRO), in which relatively short programmes were carried out with a partially-commissioned version of the instrument, having one (of four) sub-array available at each of the two bands. Unless stated otherwise, all maps and detections in this paper are at 850 μm, since this is the primary wavelength of interest for SASSy.

As part of S2SRO there were two separate sets of observations carried out for SASSy, which we now describe. The SCUBA-2 array of 32×40 transition-edge sensitive bolometers has a footprint of about 3 arcmin square on the sky (it will double in linear size when the focal plane is fully populated with sub-arrays) on the sky, and takes data at a sampling rate of approximately 200 Hz while scanning across the selected region. The available 850 μm array typically only had 50 per cent of the detectors working (although the number

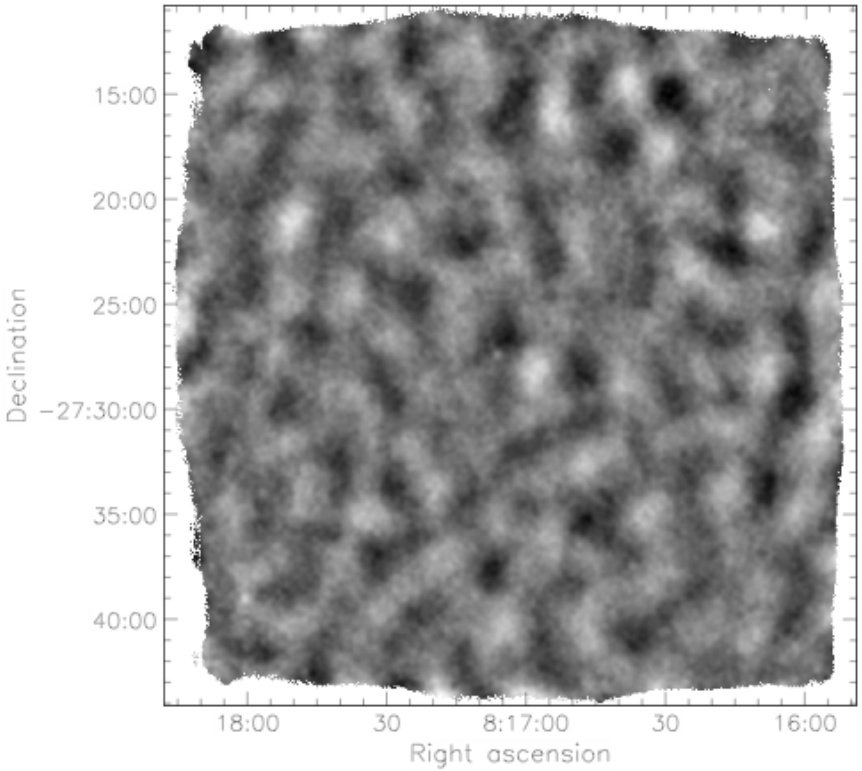

Figure 2.1: Smoothed signal-to-noise map of the 'extragalactic' field, being about 0.5° across. NGC 2559 is located at the centre of this map, which is dominated by artefacts of roughly the SCUBA-2 array size.

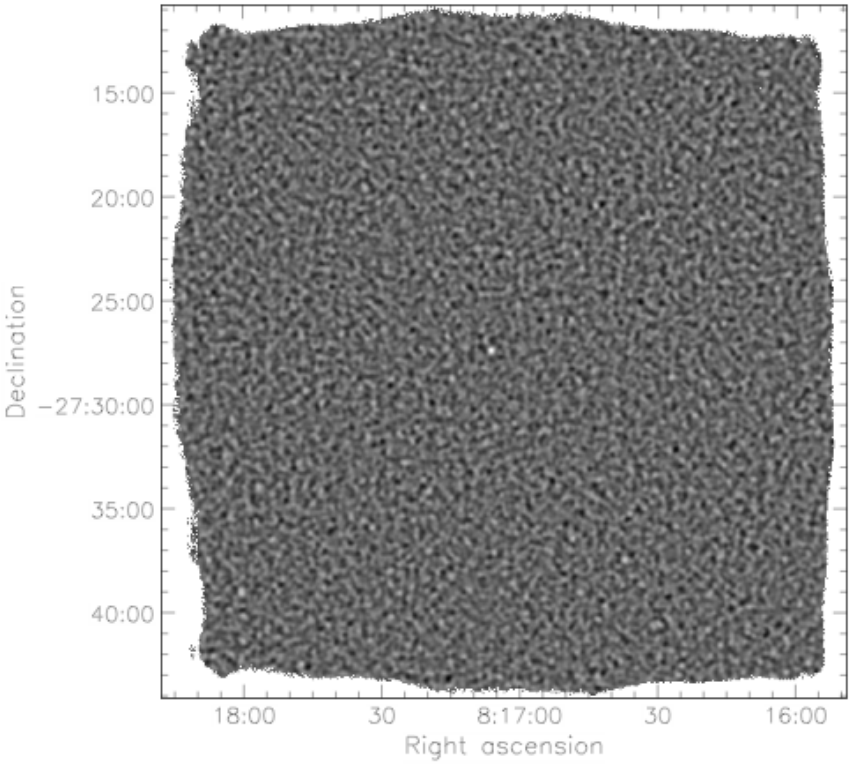

Figure 2.2: Matched-filtered signal-to-noise map of the 'extragalactic' field. NGC 2559 is located at the centre of this map, and is clearly detected. Other peaks in this map (near the north-east and south-east corners, for example) appear to be just noise excursions.

used in the data reduction is selected dynamically and hence varies with time). Calibration was performed using an internal flat-field source, as well as absolute measurements using known calibrators on the sky.

2.2.1 Extragalactic observations

The first set of observations planned was imaging of a region measuring $0.5^\circ \times 2^\circ$, with one end centred on NGC 2559, a nearby galaxy, and the other end extending into the Galactic Plane cirrus. NGC 2559 is a spiral galaxy at a distance of 20.8 Mpc (from the systemic velocity and assuming a Hubble constant of $75\,\mathrm{km\,s^{-1}}$), with morphological type SB(s)bc pec [de Vaucouleurs et al., 1991]. It was chosen as a target in this study since it is the IR-brightest nearby galaxy that lies in the SASSy area, and had not been previously observed by SCUBA. This section of sky was broken up into four $0.5^\circ \times 0.5^\circ$ tiles, of which only two were observed during the S2SRO period – these were the outer ends of the strip, and hence are not contiguous. We refer to this as the 'extragalactic' pilot survey, since (although relatively close to the Galactic Plane) the field was chosen to contain a bright *IRAS* galaxy which had not previously been observed at submillimetre wavelengths.

The region containing NGC 2559 was observed on 2010 February 27 and March 14, for a total of 167 minutes of observing, yielding an average integration time of 27 seconds per pixel. The average optical depths at 225 GHz for the two nights were $\tau_{225} = 0.097$ and 0.154, the average noise-equivalent flux densities were 160 and 260 $\mathrm{mJy\,s^{-1/2}}$, and the telescope scan rates were 240 and 360 $\mathrm{arcsec\,s^{-1}}$, respectively. Data were reduced using the SMURF map-maker (Sub-Millimetre User Reduction Facility, Chapin et al. 2010, Jenness et al. 2010b, Chapin et al. in preparation), which we describe in more detail in the next section. The resulting raw map has a noise of $38\,\mathrm{mJy\,beam^{-1}}$ determined using the produced noise map.

The region about 1° away, containing known Galactic cirrus, was observed for a total of 105 minutes, resulting in an average integration time of 16 seconds per pixel. Both 'pong' and 'rotating pong' scan strategies [Kackley et al., 2010][2] were used for the NGC 2559 field and only the rotating pong strategy for the cirrus field. Although NGC 2559 is readily detected in the resulting map of this area, we are unable to identify any Galactic

[2] 'Pong' is the default scanning mode for covering large areas with SCUBA-2, and is like a raster-scanning pattern except that it is designed to visit different parts of the map on different timescales. 'Rotating pong' means that the orientation of the pattern is allowed to rotate in sky coordinates as the observations are carried out, resulting in scans at many different angles, which is better from a map-making perspective.

cirrus within the other map. This is due to a combination of the relatively high noise level, and the difficulty in detecting extended diffuse structure (largely removed in the reduction process). Therefore for the remainder of this paper, of the two extragalactic observations, we restrict our attention to the map containing the galaxy NGC 2559.

2.2.2 Galactic observations

The second distinct set of observations targeted a field around the W5-E H II region. This region was selected because of its simple geometry and, at 2 kpc [e.g. Karr and Martin, 2003], is one of the nearest regions of triggered massive star formation [Megeath et al., 2008]. A single region of $1^\circ \times 1^\circ$ was mapped on 2009 December 5, at a speed of 600 arcsec s^{-1} (the nominal scan-rate for SASSy) using the 'pong' scanning mode [Kackley et al., 2010]. The scan pattern had each successive sweep separated by 120 arcsec, ensuring an overlap to improve mapping performance.

The on-source time was 70 minutes, which resulted in a total of 12 passes over the entire region. In addition the central $0.5^\circ \times 0.5^\circ$ was mapped at the same speed for another 70 minutes, covering that region 42 times, for a total observing time of 140 minutes. The average integration time per pixel for the inner and outer regions were 18 and 3 seconds, respectively. The 225-GHz optical depth varied from 0.08 to 0.12 with a mean of 0.10 (corresponding to Grade 3 weather). This is substantially lower than the allotted opacity band for SASSy; however, the central 0.25 deg^2 region of the map has a sensitivity slightly exceeding the SASSy target level, and therefore represents a valid test of the detectability of sources. The central portion of the map has a noise of 25 mJy $beam^{-1}$; the value for the outer region is 60 mJy $beam^{-1}$, as reported by the noise map. Note that 450 μm data were also obtained and were also reduced, but were found to be of limited use, with only the single brightest source being detected.

2.3 Data reduction and source detection

The raw time-series data were processed using SMURF [Chapin et al., 2010, Jenness et al., 2010b] called from the ORAC-DR pipeline [Gibb and Jenness, 2010]. SMURF solves for the astronomical signal using an iterative technique, fitting and filtering out noise contributions from the atmosphere and the instrument. Details of the map-maker may be found in Chapin et al. (2011, in preparation). Readings from the JCMT water-vapour monitor (WVM, Dempsey and Friberg 2008) and the values found by Dempsey [Dempsey

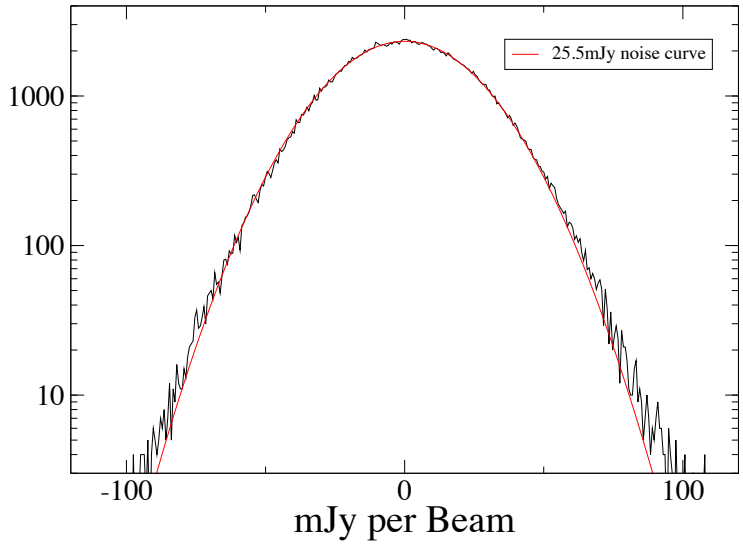

Figure 2.3: Histogram of matched-filtered pixel values in the 'extragalactic' map. This can be used to determine the spatial noise in the map. A 25.5 mJy noise curve is plotted for comparison, while the expected uncorrelated noise in the map is significantly smaller.

et al., 2010] were used to correct for atmospheric extinction. The ORAC-DR pipeline was used to mosaic the individual observations using inverse-variance weighting.

In the NGC 2559 raw map it is clear that time-dependent noise shows up as large-scale structure, obscuring the detection of the galaxy. This comes from a combination of residual sky fluctuations, as well as oscillations inherent to the instrument when these data were taken. Fig. 2.1 shows the NGC 2559 field after smoothing with the beam (to improve the signal-to-noise ratio for sources). The resulting map is dominated by structure at roughly the scale of the SCUBA-2 array. However, since the core of the galaxy shows up as a compact source, we are able to use a point source filter to make an unambiguous detection. The 'matched-filter' method implemented within ORAC-DR subtracts the map smoothed with a larger Gaussian (30 arcsec in this case) from the map convolved with a Gaussian equal to the JCMT beam-size (14 arcsec at 850 μm), thus giving a 'Mexican hat' type

spatial filter. The resulting map is able to enhance sources that are approximately point-like (since we expect extra-galactic sources found by SASSy to be approximately point-like). We experimented with different choices for filter shape, and found that the default within ORAC-DR is close to the best we can do in terms of signal-to-noise ratio. In principle we could improve things by using specific knowledge of the expected shape of NGC 2559, but that would not be helpful in a blind SASSy search (which is what we are preparing here).

Fig. 2.2 shows the NGC 2559 field after applying the matched-filter algorithm to remove the large-scale structure. NGC 2559 is now plainly visible in the centre of the map. Fig. 2.3 shows a histogram of the pixel values found in the matched-filtered map of NGC 2559. After removing the background variations in the map, the spatial noise is found to be approximately 25.5 mJy (equivalent for a point source). This is larger than the average noise of 19 mJy calculated by the data-reduction pipeline (i.e. given by the noise map), due to not having filtered out all the spatially correlated noise. Since shallow extragalactic fields should be composed of white noise plus a few sources, the signal-to-noise matched-filtered map is re-normalized to have an rms of unity before searching for sources. In other words we are effectively using the spatial rms noise, rather than the purely white noise estimate which comes from the pipeline noise map.

Fig. 2.4 shows the W5-E Galactic star-forming region map, while Fig. 2.5 shows the related signal-to-noise map and Fig. 2.5 shows an annotated version with several previously catalogued regions labelled. Since the purpose of SASSy is to find and catalogue new sources for future study, it is simplest to ignore source structure and to filter the map with the matched-filter. For objects within the Galactic strip, we use a 60 arcsec background subtraction for the matched-filter. This scale is chosen since we expect Galactic sources to be more extended than extragalactic sources. Fig. 2.10 shows the W5-E map after being matched-filtered. The central $\sim 0.5^\circ \times 0.5^\circ$ region has a spatial noise level of 15 mJy, while the outer region has a noise level of approximately 30 mJy, once processed by the matched-filter (see Fig. 2.6). Note that these values are different from the noise values in the unfiltered map since they only apply to the detection of compact sources (and so should not be considered as being a noise 'per beam', as would be usual for extended structure).

Since the matched-filters do affect the fluxes of extended sources, we have simulated extended Gaussian sources to determine the extent of this effect. Because the filter is optimized for point sources, their fluxes are unchanged. For the extragalactic matched-fileter (30 arcsec smoothed background sub-

traction), sources that appear to have a FWHM of 30 and 40 arcsec will result in a drop in peak flux by approximately 20% and 50%, respectively, after applying the matched-filter. For the Galactic matched-filter (60 arcsec smoothed background subtraction), sources that appears to have a FWHM of 60 and 80 arcsec will result in a drop in peak flux by approximately 20% and 50% respectively, after applying the matched-filter. Despite filtering out extended emission, we find that we detect many more candidate sources after applying a matched-filter than simply using the unfiltered map (27 compared with only 8). In principle, part of this increase could be due to a single extended source breaking up into multiple peaks after filtering. However, inspection of the results shows that this only happened for one source in the W5-E field. Thus for the purposes of SASSy, the matched filter offers the best method of detecting faint compact sources for followup observations.

2.4 Detections

2.4.1 NGC 2559 field

In order to extract sources from the matched-filtered maps in a manner which could be easily automated for the full survey, we use the FELLWALKER algorithm [Berry et al., 2007], implemented in the STARLINK software package CUPID. We use this algorithm simply to associate contiguous blocks of pixels with a single source – the brightness is estimated from the peak value in the match-filtered signal-to-noise map. Given the simple nature of the source detection, the choice of algorithm is not critical. A minimum number of pixels of 7 and a low RMS level are used in FELLWALKER to recover as many real and noise peaks as possible for producing histograms.

Fig. 2.7 shows a histogram of signal to noise peaks of all the sources within the NGC 2559 field. NGC 2559 is clearly detected at a signal to noise of about 7, and there are two other candidate sources at a signal to noise around 4.5. There are no obvious counterparts for these two sources in any relevant survey. The histogram shows that the detection of NGC 2559 is an outlier in the distribution, but the two other candidates seem consistent with the noise distribution, and in a map with $> 10^4$ beam-size pixels they are not very unlikely. Nevertheless we checked for counterparts in the 20-cm NVSS survey [Condon et al., 1998]. We additionally extracted archival 20-cm VLA data of approximately the same depth (lower bandwidth but larger integration time), re-reduced them and added them to the NVSS data. No radio sources are detected in the combined 20-cm image at the positions of

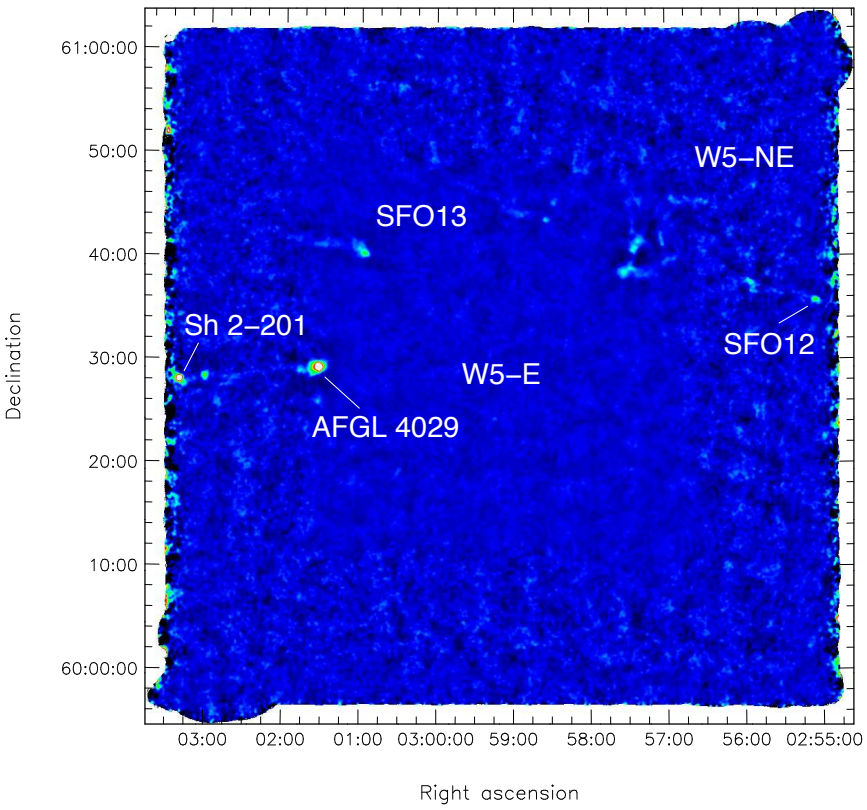

Figure 2.4: The W5-E star forming region as mapped by SCUBA-2 at 850 μm, smoothed with a Gaussian with a FWHM of 14 arcsec. The colour scale ranges from -100 to $+500\,\mathrm{mJy\,beam^{-1}}$. The central roughly 1/4 of the map can be seen to have lower noise than the rest. Known objects are labelled, as is the approximate centre of the W5-E H II region.

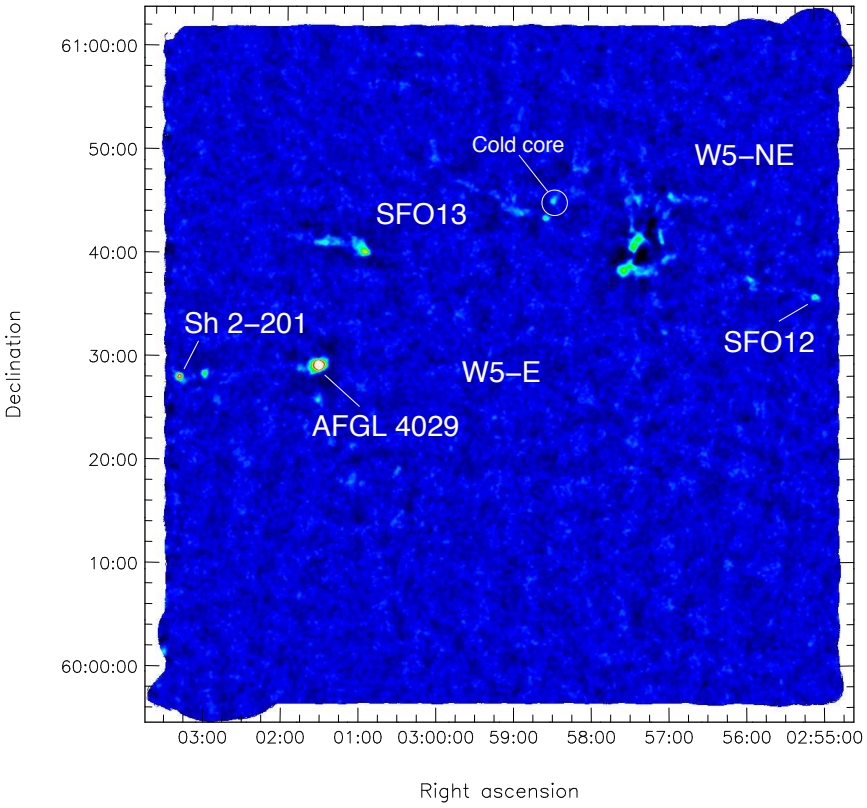

Figure 2.5: Signal-to-noise ratio image for W5-E. The colour scale ranges from −2 to +10. The 'cold core' referred to in the text is circled. Known objects are labelled, as is the approximate centre of the W5-E H II region.

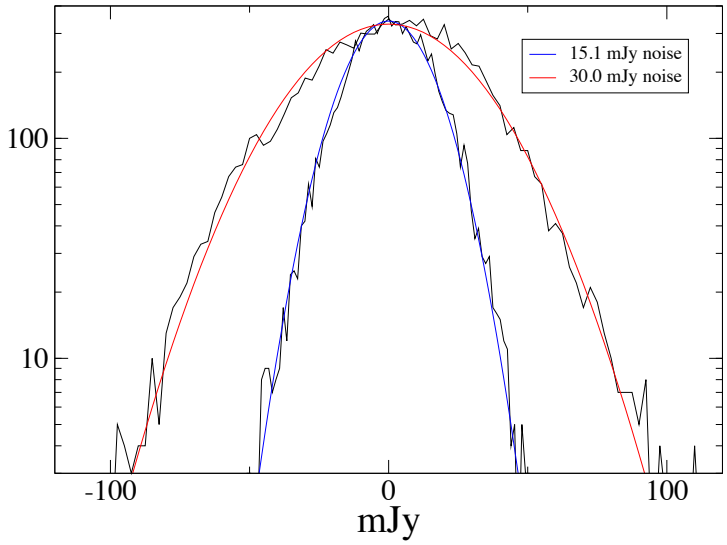

Figure 2.6: Histogram of matched-filtered pixel values in the W5-E map for 100 square pixel blank sections of the inner and outer regions of the map. Noise curves were fit and determined to be 15 and 30 mJy, respectively.

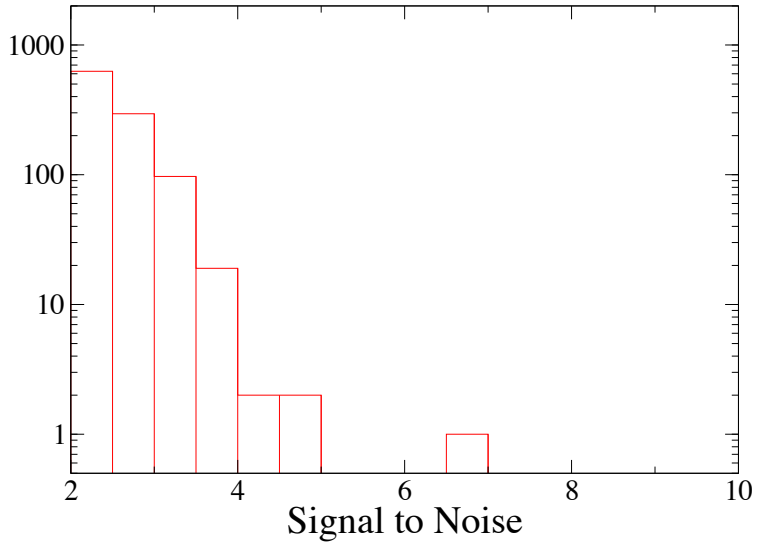

Figure 2.7: Histogram of peak signal-to-noise values within the matched-filtered NGC 2559 field. NGC 2559 itself shows up at around 6.6σ, while the 2 candidate sources at about 4.5σ appear to be noise bumps (note that a 4σ event is not very unlikely, given the number of pixels in this map).

the two peaks in the SASSy map, where the noise level is 320–350 μJy.

We also explored different choices for the filtering, and found that although the detection of NGC 2559 is robust, the next most significant peaks vary in position and brightness. The SASSy survey plan is to carry out short follow-up observations of such candidates to distinguish between real objects and false positives (whether just noise excursions or mapping artefects). This pilot survey suggests that the level at which follow-up will be worthwhile is around the 5σ level for large maps.

Fig. 2.8 shows an optical image (from the Digitized Sky Survey) of NGC 2559 with matched-filtered SCUBA-2 contours overlaid. NGC 2559 shows up at a flux density of 156 ± 26 mJy and would be detectable in data representative of SASSy (with target rms of 30 mJy).

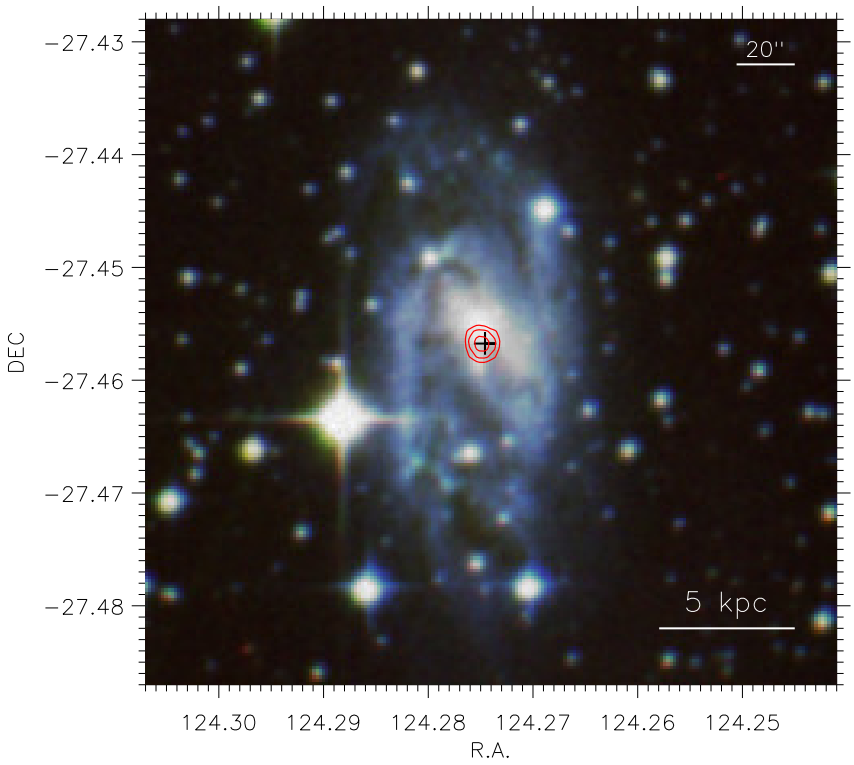

Figure 2.8: SCUBA-2 850 μm 5 and 7σ contours overlaid on an optical 3-colour image of NGC 2559 (derived from Digital Sky Survey data). The black cross marks the position of the NVSS radio source.

2.4.2 W5-E field

Turning to the Galactic pilot map, this field contains a number of known sources, including three bright-rimmed clouds (SFO 12, 13 and 14)[Morgan et al., 2008a], and the H II region Sh 2-201 [Karr and Martin, 2003]. Note that SFO 14 contains the massive young stellar object AFGL 4029. The three bright-rimmed clouds have all been detected previously at submillimetre wavelengths using SCUBA [Morgan et al., 2008b].

All of these sources are detected in the SCUBA-2 map with good to high significance. A total of 27 sources were identified at $>6\sigma$ after applying the matched-filter, most of which are unknown at submillimetre wavelengths. The central portion of the map containing the W5-E H II region is devoid of dust emission. Table 2.1 lists the objects found with a signal-to-noise ratio greater than 6 using the matched-filter method. Of the objects in Table 2.1, 11 are brighter than 150 mJy and would be detected by a blind SASSy survey at more than 5σ. Fig. 2.9 shows a histogram of signal-to-noise peaks of all the sources extracted from the W5-E map.

By inspecting the unfiltered map it is clear that some of the 'sources' found in this way are parts of extended filamentary structures. Fig 2.4 shows a number of extended, filamentary features of low signal-to-noise ratio. While faint, they are undoubtedly real, as they show good agreement with the CO data presented by Karr and Martin [2003] and Niwa et al. [2009], as well as *Spitzer* MIPS images [Koenig et al., 2008]. However, in practice, mapping such low surface-brightness features is beyond the scope of SASSy and falls into the realm of followup observations triggered by detecting new compact sources. The most interesting Galactic sources found by SASSy will be relatively isolated, and they will be discovered through applying a simple automated source-extraction procedure similar to that used here. Nonetheless it is encouraging to find that SASSy is capable of detecting extended features and there are many approaches which can be taken to characterise such morphology. Further experience with SASSy data will guide our approach.

Of all the new submillimetre detections perhaps the most striking source in the SCUBA-2 map is that labelled as the 'cold core' in Fig. 2.5. It shows up clearly in the signal-to-noise ratio map at a significance of 7σ. Comparison with *Spitzer* data reveals that while it is also detected at 160 and 70 μm, it is completely absent at 24 μm. As shown in Fig. 2.11, the SCUBA-2 source lies within the boundary of a bright-rimmed cloud, externally illuminated by the O-stars in the W5-E cluster. This source appears to be cold, a conclusion which is confirmed by our analysis below.

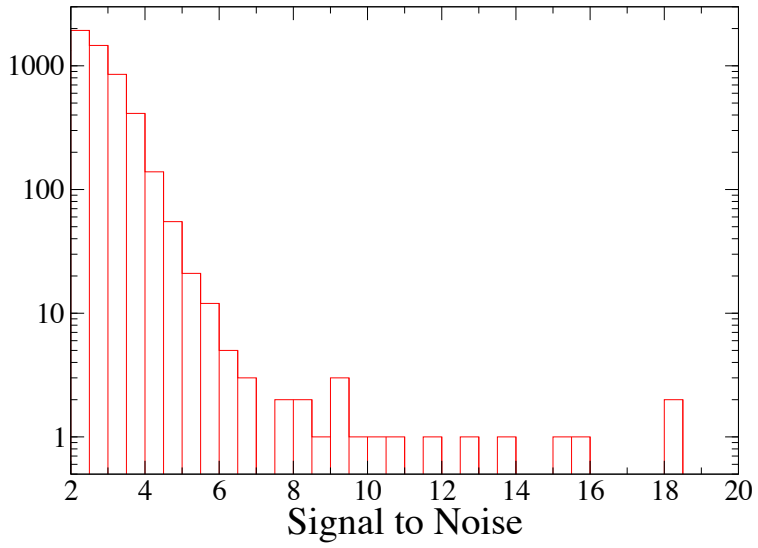

Figure 2.9: Histogram of peak signal-to-noise values within the matched-filtered W5-E field. The brightest W5-E source (AFGL 4029) has a signal-to-noise ratio of over 100 and is not shown.

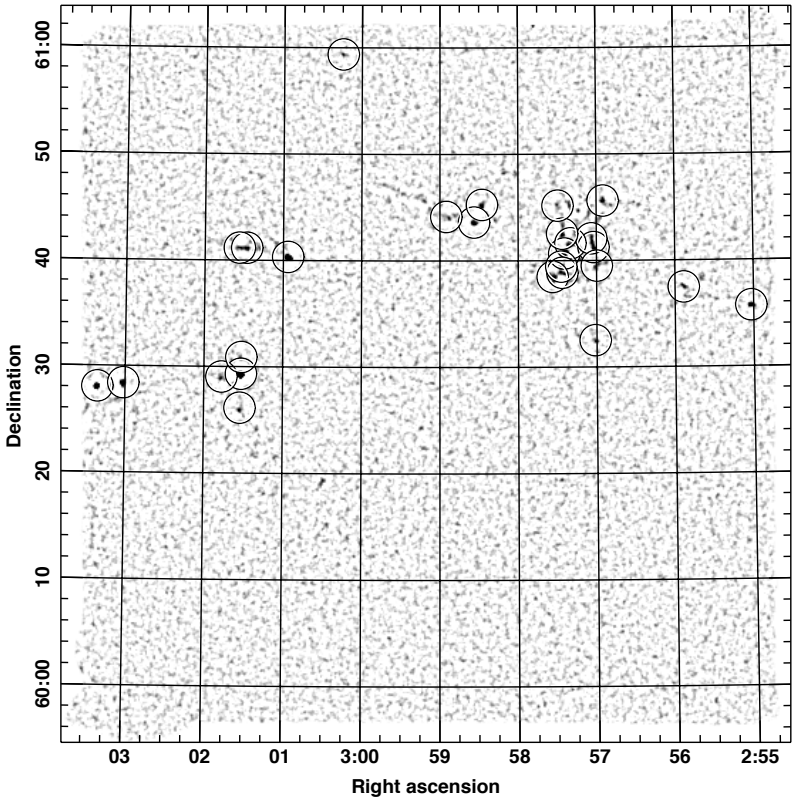

Figure 2.10: The matched-filtered map of W5-E with circles indicating the $> 6\sigma$ sources listed in Table 2.1.

S_{850}		Position (J2000)	
mJy	S/N	RA	Dec
2290	163	03:01:31.783	+60:29:19.81
1970	44.2	03:03:21.039	+60:28:03.98
410	16.0	02:55:01.806	+60:35:43.70
405	18.0	03:03:01.319	+60:28:24.23
236	18.1	03:00:56.349	+60:40:20.11
226	9.0	02:56:54.974	+60:45:37.30
212	8.6	02:55:53.335	+60:37:29.14
185	15.2	02:58:33.795	+60:43:36.67
172	12.6	02:57:02.215	+60:41:15.56
164	6.7	03:01:46.608	+60:29:03.05
152	13.8	02:57:24.688	+60:40:40.34
131	11.6	02:57:33.643	+60:38:28.77
130	6.7	03:00:14.481	+60:59:22.56
119	9.1	03:01:32.609	+60:26:08.48
118	10.5	02:58:27.730	+60:45:15.82
112	9.6	02:57:26.183	+60:38:51.92
110	8.4	02:57:03.894	+60:42:04.86
108	10.1	02:57:19.897	+60:41:37.63
99	8.2	02:57:26.221	+60:42:31.99
89	6.2	03:01:31.556	+60:30:53.96
87	7.7	02:57:27.009	+60:39:26.70
79	6.0	02:58:55.106	+60:44:08.31
77	7.7	03:01:27.812	+60:41:10.03
75	6.6	02:57:01.063	+60:32:31.05
71	6.1	02:56:59.793	+60:39:31.14
69	6.2	02:57:29.653	+60:45:10.17
68	6.2	03:01:33.497	+60:41:10.29

Table 2.1: List of objects found with a peak signal-to-noise greater than 6 in the W5-E region using the matched-filter method.

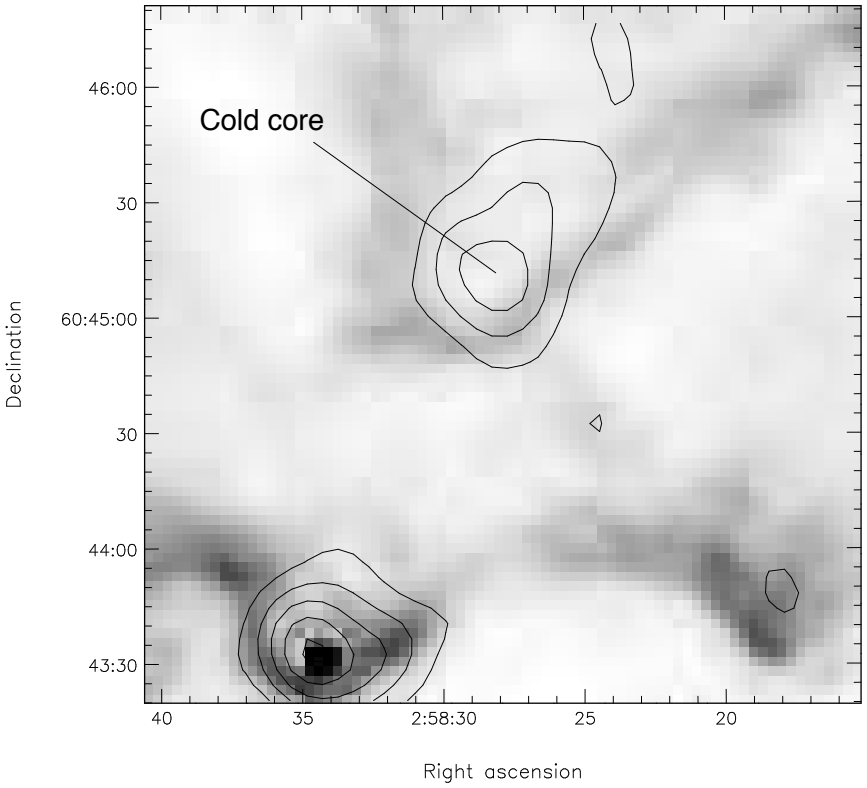

Figure 2.11: SCUBA-2 contours overlaid on *Spitzer* 24 μm image. The source labelled 'Cold core' is circled and shows up clearly in the submm, yet within a dark region of the *Spitzer* image. It is, however, detected at 70 and 160 μm with *Spitzer*.

2.5 Properties of NGC 2559

2.5.1 Ancillary data

We complement the SASSy observations of NGC 2559 with available archival mid- and far-IR data. NCG2559 has been observed by both *IRAS* and *Akari*, providing spectral coverage from 9–160 μm. These data can be used to constrain the spectral energy distribution (SED) of the source.

We estimate *IRAS* fluxes using the *IRAS* Scan Processing and Integration Tool (Scanpi [3]). Standard reduction parameters were used, taking into account the observed size of the galaxy (~ 3 arcmin, Prugniel and Heraudeau 1998; Jarrett et al. 2003) as an additional constraint. Although NGC 2559 is actually detected as a point source in all *IRAS* bands, we assume a minimum distance of 6 arcmin from the nominal position of the source for background subtraction. We obtain *Akari* fluxes at 9 and 18 μm from the *Akari*/IRC All-Sky Survey Point Source Catalogue [Ishihara et al., 2010], and at 65, 90 and 140 μm from the *Akari*/FIS All-Sky Survey Bright Source Catalogue [Yamamura et al., 2010]. We decided not to use the 160 μm measurement owing to the extremely high noise affecting this band; this is confirmed by the χ^2 increasing by about a factor 2 when this measurement is included in our fits. In addition to that, we estimate an upper limit on the 450 μm flux from the shorter wavelength SCUBA-2 map. A 20 per cent uncorrelated uncertainty is applied to all data. The observed mid- to far-IR data of NGC 2559 are shown in Table 2.2.

2.5.2 SED fitting: dust models

We fit the dust models of Draine and Li [2007] [4] to the compilation of available data. These models provide the dust emissivity per hydrogen atom, $j_\nu(q_{\rm PAH}, U_{\rm min}, U_{\rm max})$, which is a function of three parameters: the fraction of dust mass in PAHs, $q_{\rm PAH}$; the intensity of the radiation field from stars heating the interstellar medium, $U_{\rm min}$; and the intensity of the radiation field in photodissociation regions (PDRs), $U_{\rm max}$.

We apply the same general method explained in Draine and Li [2007], but we use only the seven Milky Way dust model sets, as in Wiebe et al. [2009]. Accordingly, we also set $U_{\rm max} = 10^6$ (we tested the reliability of this assumption by leaving $U_{\rm max}$ as a free parameter and found that the fit returns the same value). We thus fit to the observed SED a linear combination

[3] Available at http://scanpiops.ipac.caltech.edu/9000/applications/Scanpi/index.html
[4] Available at http://www.astro.princeton.edu/~draine/dust/dust.html .

Table 2.2: The observed SED of NGC 2559. Flux densities and respective errors are in Jy. Quoted errors include an additional 20 per cent calibration uncertainty.

λ (μm)	S_ν	δS_ν	Instrument
9	1.5	0.3	*Akari*/IRC
12	1.4	0.3	*IRAS*
18	1.8	0.4	*Akari*/IRC
25	2.8	0.6	*IRAS*
60	26	5	*IRAS*
65	23	5	*Akari*/FIS
90	39	8	*Akari*/FIS
100	66	13	*IRAS*
140	52	12	*Akari*/FIS
450	2.3	2.3	SCUBA-2 (u.l.)
850	0.156	0.04	SCUBA-2

of diffuse ISM models (with $U_{\rm max} = U_{\rm min}$) and PDR models:

$$F_\nu(q_{\rm PAH}, U_{\rm min}, U_{\rm max}) \propto \frac{M_{\rm d}}{m_{\rm H} D^2} \times [(1-\gamma) j_\nu(q_{\rm PAH}, U_{\rm min}, U_{\rm min}) + \gamma j_\nu(q_{\rm PAH}, U_{\rm min}, U_{\rm max})] ,$$

where $M_{\rm d}$ is the dust mass, $m_{\rm H}$ is the mass of a hydrogen atom and $D = 20.8\,{\rm Mpc}$ is the distance to the galaxy. We then use the derived values to evaluate the dust-weighted starlight intensity $\langle U \rangle$. The best-fit values for the parameters are found through χ^2 minimization. Fig. 2.12 shows the observed SED and best-fit curves.

We notice that the *Akari*/FIS data are systematically low with respect to the *IRAS* data. We thus evaluate the outcome of the fit using either the full data set or a subset to assess the effect of this offset. Table 2.3 summarizes the different fits and results.

Fitting the dust models to the full set of data points available yields a reasonable fit, although the χ^2 is relatively high. We obtain the values: $q_{\rm PAH} = 3.2$; $\gamma = 0.01$; $U_{\rm min} = 20$; and $\langle U \rangle = 21.9$. We derive a dust mass of $1.5 \times 10^7\,{\rm M}_\odot$ and a far-IR luminosity of $2.0 \times 10^{10}\,{\rm L}_\odot$, from which we calculate a star-formation rate of $2.8\,{\rm M}_\odot\,{\rm yr}^{-1}$ using the relation of Bell [2003]. The derived dust mass is about 2 times larger than the value obtained by Bettoni et al. [2003], who find a value of $8.3 \times 10^6\,{\rm M}_\odot$ from data at 60 and 100 μm.

Table 2.3: Draine and Li [2007] model parameters for NGC 2559 and derived physical quantities.

Data removed	None	*Akari*/FIS	*IRAS*	SCUBA-2
χ^2	17.7	10.8	10.7	3.5
degs. of freedom	7	4	3	5
$q_{\rm PAH}$	3.2	3.2	4.6	4.6
$U_{\rm min}$	20	25	20	5
$\langle U \rangle$	21.9	27.4	22.0	5.6
γ	0.01	0.01	0.01	0.01
$M_{\rm d}$ ($10^7\,{\rm M}_\odot$)	1.5	1.3	1.5	5.7
$L_{\rm FIR}$ ($10^{10}\,{\rm L}_\odot$)	2.0	2.1	1.9	2.2
SFR (${\rm M}_\odot\,{\rm yr}^{-1}$)	2.8	3.0	2.7	3.1

Note that the SFR can also be estimated using the 20 cm radio flux density along with the FIR/radio correlation (e.g. Condon 1992, Cram et al. 1998, Hopkins et al. 2001). With $S_{1.4} = 260\,{\rm mJy}$ this gives an SFR of around $10\,{\rm M}_\odot\,{\rm yr}^{-1}$, which is fairly consistent with the results obtained from the FIR fit.

Exclusion of the *Akari*/FIS data points yields again a fit which correctly matches the SCUBA-2 850 μm point. Best-fit parameters are rather similar, the only noticeable change being the increase of $U_{\rm min} = 25$ and of $\langle U \rangle = 27.4$, with the resulting dust mass, FIR luminosity and SFR fairly consistent with the previous fit.

Removing the *IRAS* points from the data set yields a similar fit with a χ^2 of 10.7 with 3 degrees of freedom. The fit parameters are almost undistinguishable from the first fit at $\lambda \geq 30\,\mu$m.

For comparison, we also fit the models after excluding the SCUBA-2 point and upper limit. We obtain lower values of $U_{\rm min} = 5$ and $\langle U \rangle = 5.6$. But now the best-fit misses the 850 μm flux density by about a factor 4.

This shows the strong leverage of the SCUBA-2 data to properly constrain the FIR and sub-mm SEDs of galaxies. In particular, in addition to the dust mass, the value of the starlight intensity $U_{\rm min}$ (and consequently $\langle U \rangle$) is strongly sensitive to the 850 μm flux density.

2.5.3 SED fitting: modified blackbody

For comparison with the more detailed Draine and Li [2007] models, we also fit a modified blackbody spectrum to the observed data. The fit is carried out assuming a shape for the modified blackbody described by the

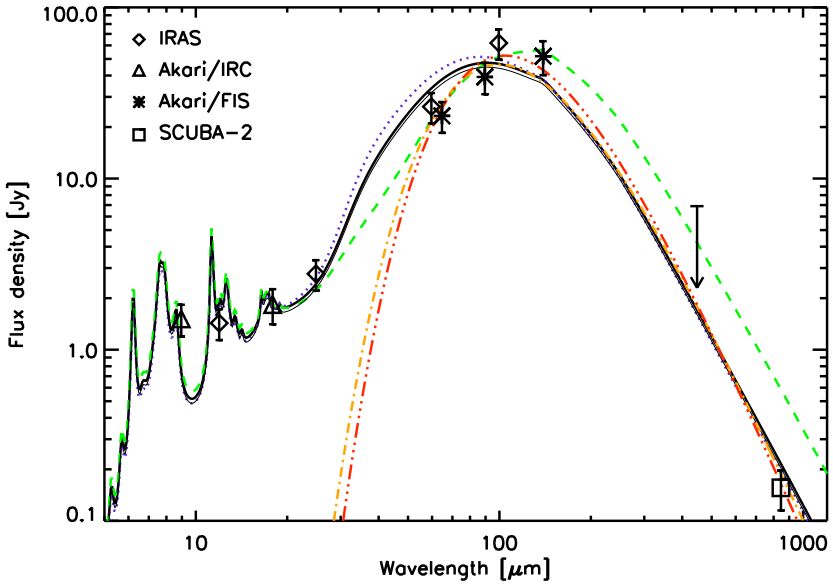

Figure 2.12: The observed far-IR and sub-mm SED of NGC 2559, together with dust model fits. An arrow marks the 3σ upper limit at 450 μm. The solid (black) line shows the best fit to all available data points. The dotted (blue) line is the best fit to the dataset excluding the *Akari*/FIS data. The thin solid (black) line is the best fit to the dataset excluding the *IRAS* data. The dashed (green) line is the best fit model without the SCUBA-2 points. The dot-dashed (orange) line is the modified blackbody fit with $\beta = 2$. The triple-dot-dashed (red) line is the modified blackbody fit with free β. Error bars include an uncorrelated 20 per cent uncertainty.

Table 2.4: Modified blackbody fits for NGC 2559 and derived physical quantities.

Fit	χ^2	degs. of freedom	β	$T_{\rm d}$ (K)	$M_{\rm d}$ ($10^7\,{\rm M}_\odot$)	$L_{\rm FIR}$ ($10^{10}\,{\rm L}_\odot$)	SFR (${\rm M}_\odot\,{\rm yr}^{-1}$)
Fixed β	6.0	5	2	29	0.31	1.8	2.6
Free β	4.7	4	2.3	26	0.47	2.0	2.8

expression

$$S_\nu = \frac{M_\mathrm{d}\kappa}{D^2}\left(\frac{\nu}{\nu_0}\right)^\beta B_\nu(T), \tag{2.1}$$

where $\nu_0 = 1.2\,\mathrm{THz} = c/(250\,\mu\mathrm{m})$, κ is the dust mass absorption coefficient at ν_0, β is the dust emissivity index and M_d is the dust mass. Once again, the best-fit parameters are found by χ^2 minimization. We assume a mean value of $\kappa = 0.29\,\mathrm{m^2\,g^{-1}}$ (see e.g. Wiebe et al. 2009, although there is considerably uncertainty in this value) and fix $\beta = 2$.

This modified blackbody fit yields consistent values of M_d, L_FIR and SFR with respect to the detailed dust models. Table 2.4 summarizes the modified blackbody results, and the fitted curves are shown in Fig. 2.12. We see that the dust temperature of NGC 2559 is around 26–29 K. This is warmer than for most of the galaxies studied in the SINGS sample [Draine et al., 2007], as well as those studied using BLAST [Wiebe et al., 2009]. This is consistent with requiring a relatively higher value of U than for those other galaxies.

2.6 Source properties in W5-E

From our catalogue of compact sources within the W5-E region we select two example sources, representative of two extreme regimes: (i) the brightest source in the field, AFGL 4029 (Deharveng et al. 1997 and references therein); and (ii) a fainter source to the NW of the first, as an example of a potentially colder core (labelled 'cold core' in Fig. 2.5). The SCUBA-2 flux densities for both sources were obtained from photometry within an aperture of 30-arcsec diameter.

Ancillary data available for this region include *Spitzer* MIPS 70 μm observations of the whole field, as well as *IRAS*, *Akari* coverage, and SCUBA imaging for part of the field. The SCUBA-2 data are in excellent agreement with the SCUBA measurements, being consistent within errors, but covering a much wider area. We show *Spitzer* 70μm contours on top of the SCUBA-2 image in Fig. 2.13.

The bright source AFGL 4029 is detected in almost all wavebands, having upper limits only at 65 and 90 μm. We fit a modified blackbody spectrum to the observed SED, after adding a 20 per cent uncorrelated uncertainty to the errors, as we did for NGC 2559. Leaving β as a free parameter in the fit yields a value of $\beta = 2.02$, which suggests that $\beta = 2$ is a good assumption for the dust emissivity index. We derive a temperature $T = 31$ K and a dust

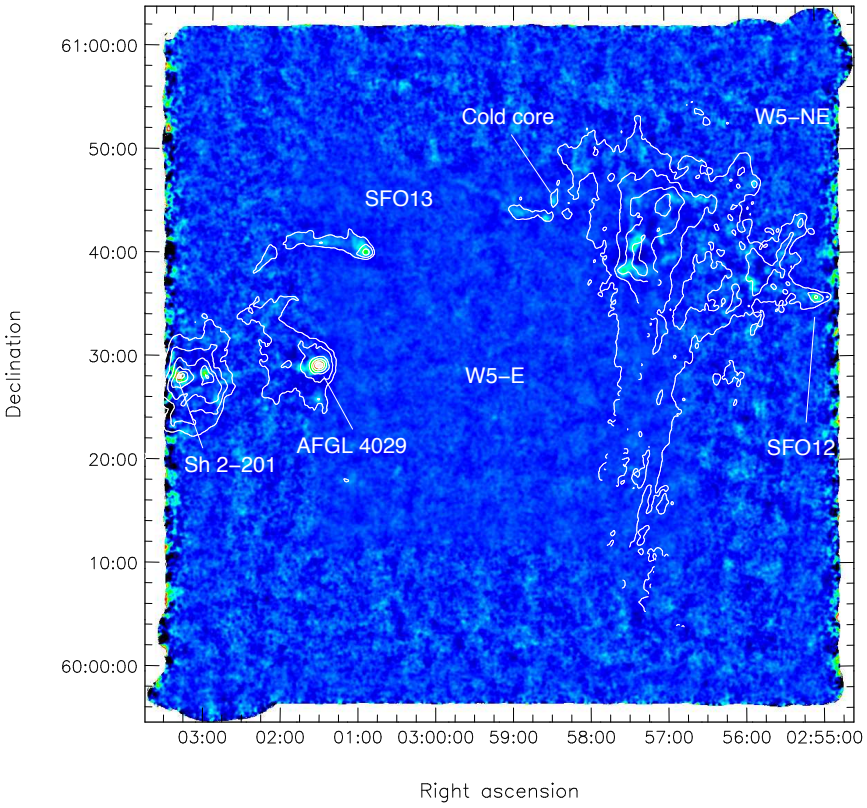

Figure 2.13: SCUBA-2 850 μm emission in colour with *Spitzer* 70 μm contours overlaid. Sources are labelled as in Fig. 2.4. The *Spitzer* contours do not close to the south of W5-NE due to a lack of coverage there.

mass of $60\,M_\odot$, with a FIR luminosity of $5000\,L_\odot$. This is in reasonable agreement with the value of $3200\,L_\odot$ estimated by Morgan et al. [2008b].

The faint source is detected only at 70 and 850 μm. A relatively nearby 90 μm source is detected by *Akari*, however its position is offset by 28 arcsec from the *Spitzer* position. Although this lies within the PSF of *Akari* at 90 μm, we prefer not to use this measurement in our analysis to avoid contamination by other potential sources (and in any case it adds little to the 70 μm constraint). Reliable flux densities were obtained from the *Spitzer* 24 and 70 μm images, using the same 30-arcsec aperture as for the SCUBA-2 data. While the cold core is also evident in the 160 μm MIPS image, the presence of significant artefacts prevents the extraction of a useful flux density measurement.

Although only two photometry points are available, a fit to the SED using again a modified blackbody with $\beta = 2$ yields reasonable quantities and confirms this source to be a cold protostellar core. We obtain a temperature $T = 17\,K$, FIR luminosity of $27\,L_\odot$ and a dust mass of $11\,M_\odot$. Comparing the *Akari* 90 μm point to the fit shows that the measurement is in excellent agreement with the expected flux density, suggesting that this might actually be the counterpart to the same source. The result of the fit for both sources is shown in Fig. 2.14.

The readiness with which we were able to pick out a relatively cold source, even in this small pilot study, shows that SASSy will be able to detect single low-mass cold clumps inside larger star-forming regions. Detailed follow-up of such sources will determine where they lie on the star-formation sequence.

2.7 Discussion

With the current SASSy S2SRO observations, we have shown that we will be able to detect and catalogue real sources, both Galactic and extragalactic. Based on early commissioning estimates, SCUBA-2 mapping during S2SRO was expected to be approximately 50 times faster than for SCUBA. A direct comparison with the SCUBA data in the W5-E field shows the mapping speed improvement factor to be 60, after scaling the map sizes and noise levels. Assuming similar weather conditions and a similar efficiency for the new science-grade arrays currently being commissioned on SCUBA-2, SASSy should be able to map the sky at a rate of $> 0.8\,deg^2$ per hour to the target sensitivity, exceeding the capabilities of SCUBA by hundreds of times. The current estimate for the Noise Equivalent Flux Density (NEFD) is given by,

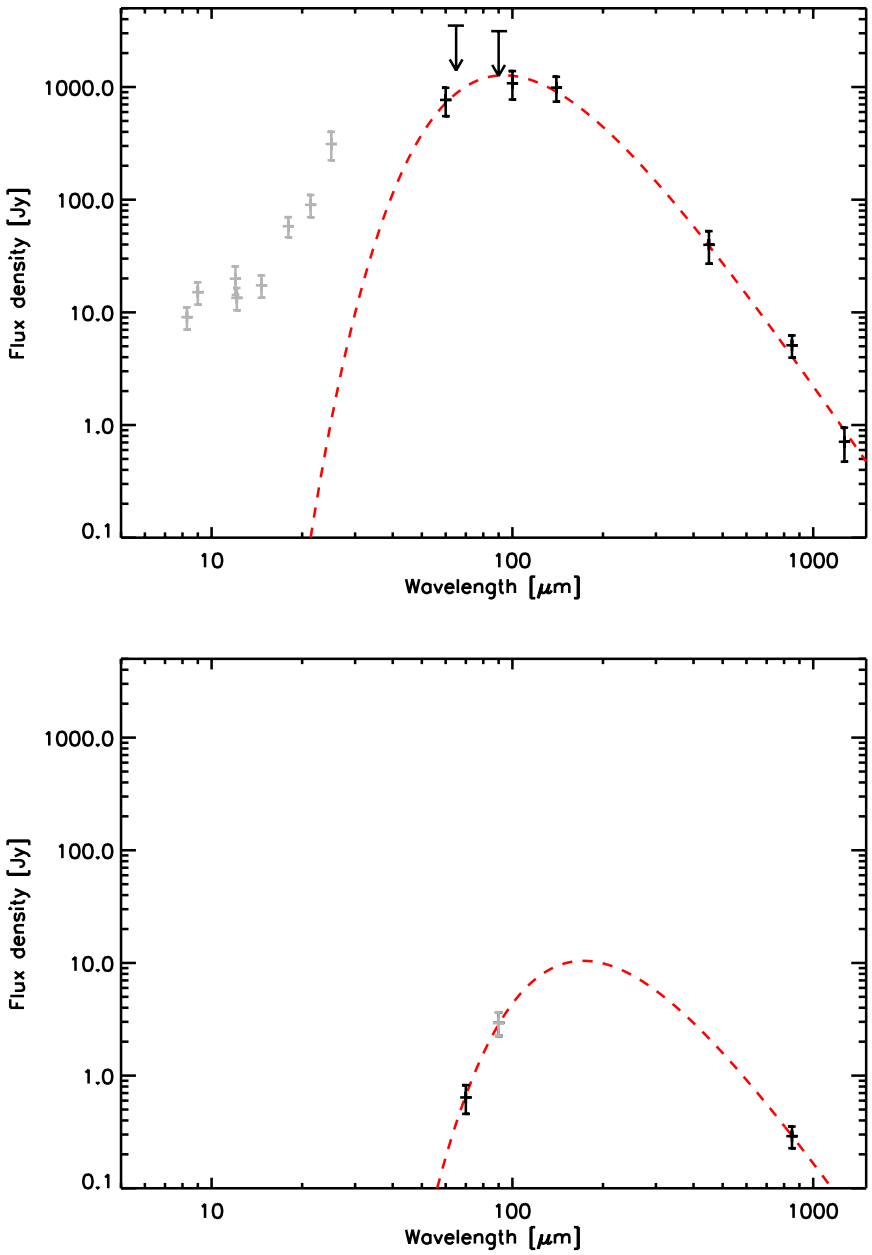

Figure 2.14: The observed far-IR and sub-mm SED of AFGL 4029 and of the cold source in W5-E. Black points are used for the fit, arrows mark upper limits. The dotted (red) line is the modified blackbody fit with $\beta = 2$.

$$NEFD_{850} = \left(\frac{70}{T_{850}} - 5\right) \frac{1}{\sqrt{3630}} mJy\sqrt{s},$$

where T_{850} is the atmospheric transmission at 850 μm. Currently, all four arrays at each wavelength have been installed, undergone commissioning, and the first call for proposals for science has been made.

These initial data have shown that it is possible to reach a 1σ sensitivity to point sources of ~ 30 mJy while scanning rapidly with SCUBA-2 in relatively mediocre weather conditions. The map-making and source extraction procedures are fast and require little in the way of human intervention. Experience with this pilot programme has already been fed back directly into the software pipeline and most of the data processing and analysis is now automated.

The science case for SASSy remains strong and has been made stronger by recent *Herschel* discoveries. There is still a pressing need for a wide-area shallow 850 μm survey in the era of *Herschel*, *Planck* and ALMA. This pilot study has shown that it is feasible to find sources in the shallow maps which SCUBA-2 will soon produce routinely.

Chapter 3

Disentangling a lensed group of galaxies at z=2.9 observed with SCUBA-2

3.1 Introduction

MS 0451.6−0305 is galaxy cluster at a redshift of 0.5386. The massive cluster is lensing several background sources and has been imaged at many different wavelengths: radio [Reese et al., 2000, Berciano Alba et al., 2010]; millimetre/submillimeter [Borys et al., 2004, Wardlow et al., 2010]; far-IR (part of HerMES); mid-IR [Geach et al., 2006]; near-IR [Borys et al., 2004, Wardlow et al., 2010]; optical [Gioia and Luppino, 1994, Moran et al., 2007, Kodama et al., 2005]; and X-ray [Donahue et al., 2003]. In the optical the lensed objects include an extended arc as well as two extremely red objects (EROs) and a Lyman-break galaxy (LBG) [Borys et al., 2004]. The two EROs and the LBG are at a redshift of approximately 2.9 and possibly constitute an interacting system [Borys et al., 2004]. At 850 μm SCUBA showed a 'giant submm arc', consistent with the merging of several galaxies which lie near the critical line in the lens model. Several millimeter sources have also been identified in the surrounding region by Wardlow et al. [2010] using AzTEC. Fig. 3.1 illustrates the complicated nature of this lens.

The cluster was recently observed with SCUBA-2 during commissioning of the instrument in late 2009 as part of 'Guaranteed Time'. The observations lasted for approximately 7 hours. Since the lens had already been observed at 850 μm using SCUBA, the motivation for the new observations were: (1) to confirm the bright lensed structure with SCUBA-2, without the complications introduced by SCUBA's requirement to chop; (2) to detect the lensed structure at 450 μm, with resolution better by about a factor of two; and (3) to make a larger image going well beyond the core of the cluster, perhaps enabling detection of the Sunyaev-Zeldovich effect, as well as enhanced star-formation in in-falling galaxies. The images were taken in

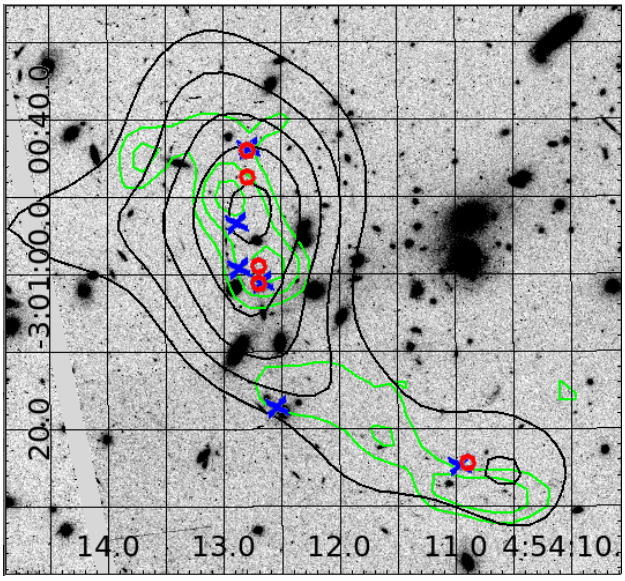

Figure 3.1: *HST* image of MS 0451−03 with SCUBA-2 850 μm contours (black), SCUBA-2 450 μm contours (green), two multiply imaged EROs (red cicles), an optical arc comprising of a multiply imaged LBG (more obvious in right hand figure), and radio sources detected by [Berciano Alba et al., 2010] (blue crosses).

weather which was good enough to obtain 450 μm detections, with the hope of breaking up the arc into sources. The size of the new map (made with one sub-array at each wavelength) is about an order of magnitude larger in area than the SCUBA image, but still not large enough to encompass the entire cluster. The new 450 μm data can also be used to crudely constrain the spectral energy distributions of detected sources, at least distinguishing galaxies in the cluster ($z \sim 0.5$) from those in the lensed background region ($z \sim 3$).

3.2 SCUBA-2 data

The images were made using the iterative map-maker (Chapin et al., in prep.) within SMURF [Jenness et al., 2010a]. Currently, the most reliable method of detecting compact sources is to apply a 'Mexican hat' type spatial filter to remove large scale structure. This technique is described in detail in Chapter 2. Note that we also tried to improve the map in the region of the 'submm arc' by using a masking procedure within the map-maker; however, we were unable to produce significantly better results. Additionally we added the SCUBA map of Borys et al. into the data at the time-stream level (at a randomly selected position away from the centre of the SCUBA-2 image), in an effort to determine the spatial filtering introduced by the map-maker. In fact we found very little effect on the scales of the emission described in Borys et al. (2004), and so we expect the map shown in the left panel of Fig. 3.2.1 to be a fairly accurate representation of the lensed source(s). The extent to which the morphology appears to be different is probably largely the effect of noise (which is clearly spatially correlated).

3.2.1 850 μm maps

At 850 μm, the 'submm arc' is easily detected by SCUBA-2. It is elongated roughly north-south, just as in the earlier SCUBA image. Since the field is larger, there are a handful of additional sources also detected. These new 850 μm sources are mostly coincident with known AzTEC 1.1-mm sources. The left panel of Fig. 3.2.1 shows a false colour image of the SCUBA-2 map with contours from the SCUBA map [Borys et al., 2004] overlaid. In the right panel we have applied a filter to extract point sources (see MacKenzie et al. [2011]) to suppress large scale correlations in the image while pulling out sources of order the beamsize. Looking at this map, we see that the source to the east of the centre, labelled 'P' by Borys et al. (2004), is also detected at about 6σ [Borys et al., 2004]. The circles on this map show

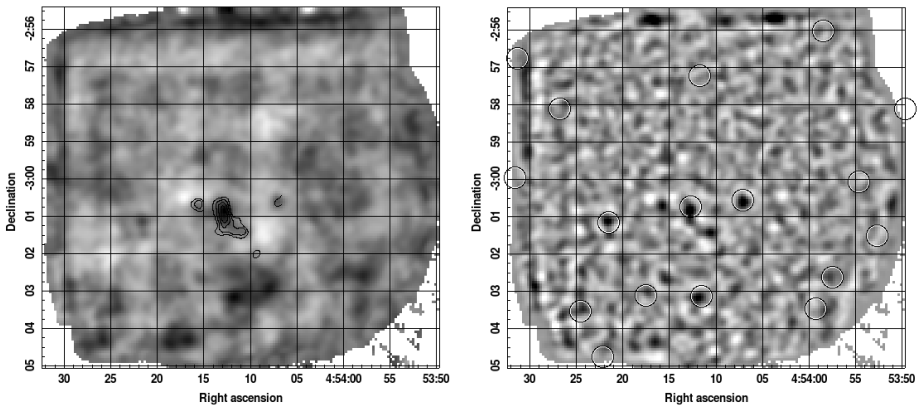

Figure 3.2: Left: The 850 μm signal map with original SCUBA contours overlaid [Borys et al., 2004]. Right: The 850 μm matched-filtered signal map with AzTEC sources circled [Wardlow et al., 2010]. The matched-filtered map has 0.9 mJy per beam noise at the position of the lens.

the positions of all sources detected by AzTEC [Wardlow et al., 2010] – this does not include 'P', but does include a source at the cluster redshift (further to the east, labelled AzTEC source 5 by Wardlow et al.), another which appears to be in the foreground (west of the lensed sources, AzTEC source 10) and one at moderate redshift behind the cluster (to the south of the centre, AzTEC 18).

3.2.2 450 μm maps

Several of the observations at 450 μm are of poor quality and suffer from spikes or jumps in the bolometer time streams. This results in maps that are filled with stripes. These observations are not used when creating the current SCUBA-2 maps. The mapping is also problematic due to there being artificial large scale structure introduced into the map by correlated noise in the bolometer signal time-stream. The extended lensed structure appears to be detected (see Fig. 3.2.2), but it is difficult to decide how much it is affected by artificial large scale structure at that location. Once matched-filtered, the lens appears to break up into two sources, with signal-to-noise ratios (SNRs) of 3.6 and 3.7, for the component to the north and south-west, respectively. These SNR values are estimated using the noise map which comes from the iterative map-maker. However, if we examine the spatial variation in the signal map we come up with a different noise

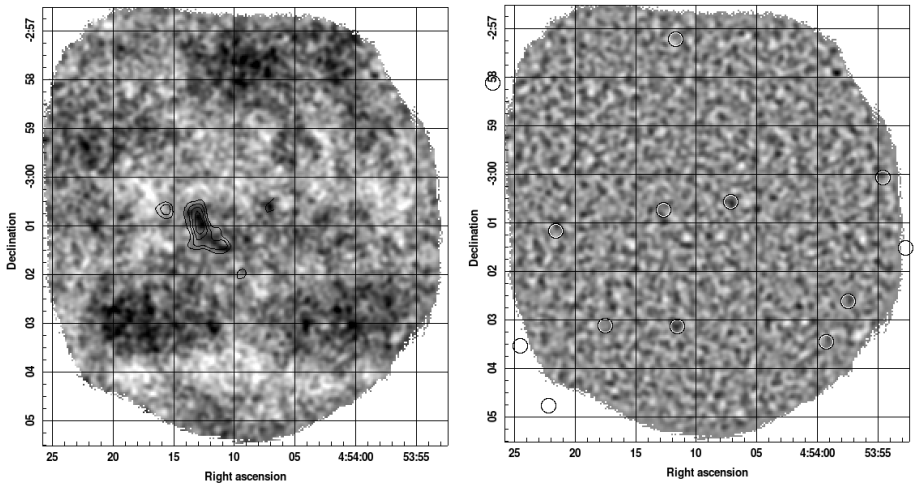

Figure 3.3: Left: The 450 μm map with SCUBA-2 850 μm contours overlaid. Right: The 450 μm matched-filtered signal-to-noise map with AzTEC sources circled [Wardlow et al., 2010]. The matched-filtered map has 4.1 mJy per beam noise at the position of the lens.

estimate, which is somewhat higher (including probably some artefacts, as well as confusion) – using this noise estimate the two components of the 'submm lens' become 3.3σ and 3.4σ detections.

Also detected, are two of the AzTEC sources – source 18 and 10 [Wardlow et al., 2010] at 3.5σ and 4.0σ, respectively. These are identified with galaxies at $z \sim 0.3$ and $z \sim 0.7$, so their detection at 450 μm is entirely consistent.

The morphology of the lens at 450 μm appears different from what might have been expected based on existing observations. Splitting the observations into two separate maps yields somewhat different morphologies, although this might simply be attributed to the low SNR detections (expected values of approximately 2.6 for both sources in each individual half map).

3.3 Comparison with previous data

3.3.1 Identified lensed sources

Previous studies of the central region of this cluster have shown strong lensing, with different lensed images identified in different wavebands. For comparison purposes, the sources detected in the three previous studies in the

submillimeter and radio are overplotted onto the new 450 μm and 850 μm data. Fig. 3.3.1 compares sources found by: Borys et al. (2004, upper panel); Berciano et al. (2007, middle panel); and Berciano et al. (2010, lower panel). Other than a general consistency with the positions of the already identified lensed images, it is unclear how much SCUBA-2 can currently add to the already complicated lensing story.

3.3.2 Stacking results

As a reality check, as well as to test for artefacts or offsets in the SCUBA-2 data, we have performed a 'stack' at the position of a catalogue of 24 μm sources detected with *Spitzer* MIPS in this field [Geach et al., 2006]. We simply took a square section of the SCUBA-2 image at each position and performed a straight average. Fig. 3.3.2 shows the 850 μm and 450 μm stacked images, which are certainly positive in the centre, with no obvious astrometry offsets.

3.3.3 Mid-IR and radio

Fig. 3.3.3 shows the comparison between the MIPS 24 μm image, VLA 1.4 GHz map from Berciano Alba et al. [2010], and the 450 μm map. It is clear that there is a high degree of correlation between the 450 μm data and the IR and Radio, and with higher signal-to-noise at 450 μm a detailed comparison could be made.

3.3.4 AzTEC sources

A 1.1-mm AzTEC survey of the MS0451.6 cluster and surrounding region was described by Wardlow et al. [2010]. It is difficult to reconstruct faint large scale structure from AzTEC data. In practice the data are time-stream filtered using a Principle Component Analysis approach, and then the resulting maps are spatially-filtered with a Wiener filter. This means that AzTEC images are more severely filtered than images from SCUBA-2, and hence the basic SCUBA-2 maps (at both wavelengths) show more evidence for the 'submm arc' than was seen by AzTEC.

After applying the matched filter to the SCUBA-2 images, we arrive at maps which are well suited for comparison with the AzTEC image, since both have been processed in order to pull out compact sources. Another advantage with comparing directly to the AzTEC study is that Wardlow et al. [2010] has already identified counterparts for many of their sources.

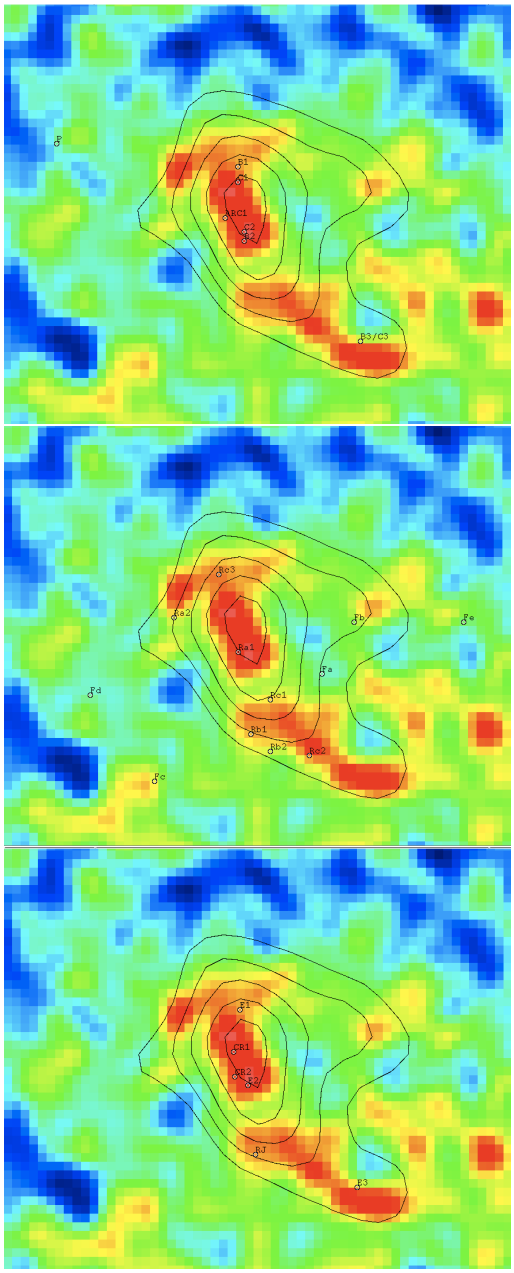

Figure 3.4: Comparison of the new 450 μm (colour image) and 850 μm (contours) SCUBA-2 data with lensed sources identified by Borys et al. (2004) (top) [Borys et al., 2004], Berciano et al. (2007) (middle) [Berciano Alba et al., 2007], and Berciano et al. (2010) (bottom) [Berciano Alba et al., 2010].

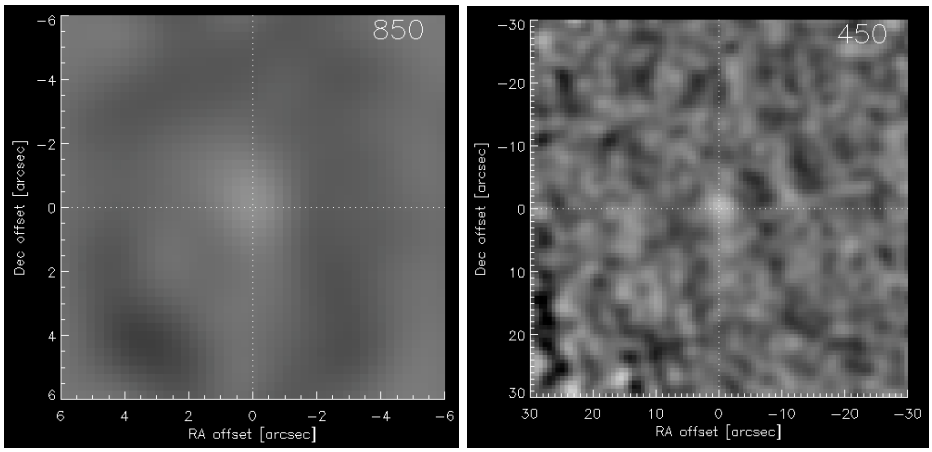

Figure 3.5: Resulting 850 μm (left) and 450 μm (right) stack on the positions of 24 μm MIPS sources.

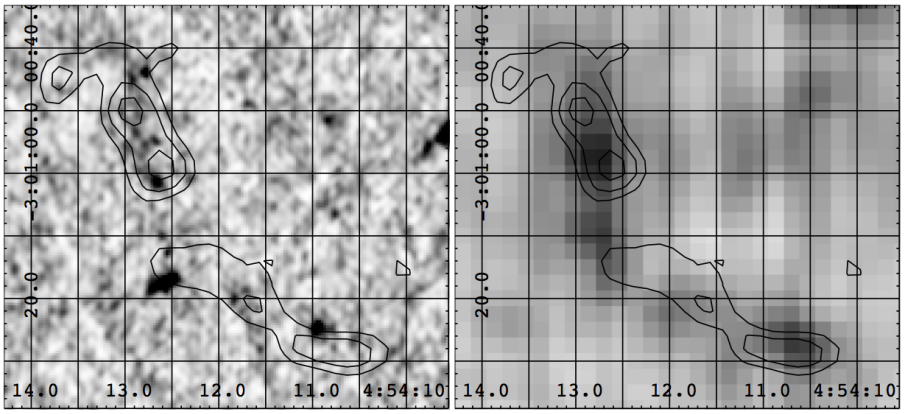

Figure 3.6: Left: 1.4 GHz VLA image with 450 μm contours overlaid. Right: 24 μm MIPS image data with 450 μm SCUBA-2 contours overlaid.

For these reasons we have been focussing on what we can do with the combination of 2-band SCUBA-2 data with photometry at slightly longer wavelengths using AzTEC.

There are five 850 μm and two 450 μm sources (other than the lens detected by SCUBA-2) that were also identified by AzTEC. Three of these sources have redshift estimates, with one source being a possible cluster member, one in the foreground and one in the background. With these new data, we should be able to fit modified blackbody spectra, as well as refine redshift estimates.

3.3.5 ALMA cycle 0 proposal

The Atacama Large Millimeter/Sub-millimeter Array (ALMA) is a new interferometer currently undergoing commissioning in Chile. The first call for proposals ended in June of 2011 with the intention of using 16 of its 12 meter antennae in both a compact and an extended configuration. Its high sensitivity and high resolution make it perfect for resolving the submillimeter lens and can even observe at the same wavelengths as SCUBA-2. For this reason, we have submitted a proposal to observe the lens using ALMA. This proposal is found in appendix A.

Bibliography

E.F. Bell. Estimating Star Formation Rates from Infrared and Radio Luminosities: The Origin of the Radio-Infrared Correlation. *ApJ*, 586:794, 2003.

A. Berciano Alba, M. A. Garrett, L. V. E. Koopmans, and O. Wucknitz. Highly-magnified, multiply-imaged radio counterparts of the sub-mm starburst emission in the cluster-lens MS0451.6-0305. *A&A*, 462:903–911, February 2007. doi: 10.1051/0004-6361:20065223.

A. Berciano Alba, L. V. E. Koopmans, M. A. Garrett, O. Wucknitz, and M. Limousin. Radio counterpart of the lensed submm emission in the cluster MS0451.6-0305: new evidence for the merger scenario. *A&A*, 509: A54, January 2010. doi: 10.1051/0004-6361/200912903.

D.S. Berry, K. Reinhold, T. Jenness, and F. Economou. In R.A. Shaw, F. Hill, D.J. Bell, editor, *Astronomical Data Analysis Software and Systems XVI*, volume 376 of *ASP Conf. Ser*, page 425, 2007.

D. Bettoni, G. Galletta, and S. García-Burillo. A new catalogue of ISM content of normal galaxies. *A&A*, 405:5, 2003.

C. Borys, S. Chapman, M. Donahue, G. Fahlman, M. Halpern, J.-P. Kneib, P. Newbury, D. Scott, and G. P. Smith. The nature of a gravitationally lensed submillimetre arc in MS0451.6-0305: two interacting galaxies at z˜ 2.9? *MNRAS*, 352:759–767, August 2004. doi: 10.1111/j.1365-2966.2004.07982.x.

E. Chapin, A.G. Gibb, T. Jenness, D.S. Berry, and D. Scott. *The Sub-Millimetre User Reduction Facility, Starlink User Note 258, Version 1.0.0,* `http://www.starlink.ac.uk/docs/sun258.htx/sun258.html`. 2010.

J. Clarke and A. I. Braginski. *The SQUID Handbook: Fundamentals and Technology of SQUIDs and SQUID Systems*. Wiley-VCH, 1 edition, August 2004. ISBN 3527402292.

J.J. Condon. Radio emission from normal galaxies. *ARA&A*, 30:575, 1992.

J.J. Condon, W.D. Cotton, E.W. Greisen, Q.F. Yin, R.A. Perley, G.B. Taylor, and J.J. Broderick. *ApJ*, 115:1693, 1998.

L. Cram, A. Hopkins, B. Mobasher, and M. Rowan-Robinson. Star Formation Rates in Faint Radio Galaxies. *ApJ*, 507:155, 1998.

Gary Davis, Michel Fich, Mark Halpern, Doug Johnstone, Brenda Mattews, Gerald Moriarty-Shieven, Rene Plume, and Douglas Scott. James clerk maxwell telescope (jcmt) and scuba-2: Submission to the long range plan. 2010. www.casca.ca/lrp2010/Docs/LRPReports/LRP_JCMT.pdf.

G. de Vaucouleurs, A. de Vaucouleurs, H.G. Corwin, Jr., R.J. Buta, G. Paturel, and P. Fouque. *Third Reference Catalogue of Bright Galaxies*. Springer-Verlag, Berlin, 1991.

L. Deharveng, A. Zavagno, I. Cruz-Gonzalez, L. Salas, J. Caplan, and L. Carrasco. AFGL 4029: a cluster of massive young stars. *A&A*, 317: 459, 1997.

J. T. Dempsey, P. Friberg, T. Jenness, D. Bintley, and W. S. Holland. Extinction correction and on-sky calibration of SCUBA-2. 7741, July 2010. doi: 10.1117/12.856476.

J.T. Dempsey and P. Friberg. *SPIE*, 7012:137, 2008. doi: 10.1117/12.787471.

J. Di Francesco, D. Johnstone, H. Kirk, T. MacKenzie, and E. Ledwosinska. The SCUBA Legacy Catalogues: Submillimeter-Continuum Objects Detected by SCUBA. *ApJS*, 175:277–295, March 2008. doi: 10.1086/523645.

M. Donahue, J. A. Gaskin, S. K. Patel, M. Joy, D. Clowe, and J. P. Hughes. The Mass, Baryonic Fraction, and X-Ray Temperature of the Luminous, High-Redshift Cluster of Galaxies MS 0451.6-0305. *ApJ*, 598:190–209, November 2003. doi: 10.1086/378688.

B. T. Draine, D. A. Dale, G. Bendo, K. D. Gordon, J. D. T. Smith, L. Armus, C. W. Engelbracht, G. Helou, R. C. Kennicutt, Jr., A. Li, H. Roussel, F. Walter, D. Calzetti, J. Moustakas, E. J. Murphy, G. H. Rieke, C. Bot, D. J. Hollenbach, K. Sheth, and H. I. Teplitz. Dust Masses, PAH Abundances, and Starlight Intensities in the SINGS Galaxy Sample. *ApJ*, 663: 866, 2007.

B.T. Draine and A. Li. Infrared Emission from Interstellar Dust. IV. The Silicate-Graphite-PAH Model in the Post-Spitzer Era. *ApJ*, 657:810, 2007.

J. E. Geach, I. Smail, R. S. Ellis, S. M. Moran, G. P. Smith, T. Treu, J.-P. Kneib, A. C. Edge, and T. Kodama. A Panoramic Mid-Infrared Survey of Two Distant Clusters. *ApJ*, 649:661–672, October 2006. doi: 10.1086/506469.

A.G. Gibb and T. Jenness. *Processing SCUBA-2 Data with ORAC-DR, Starlink User Note 264, Version 1.0.0,* `http://www.starlink.ac.uk/docs/sun264.htx/sun264.html`. 2010.

I. M. Gioia and G. A. Luppino. The EMSS catalog of X-ray-selected clusters of galaxies. 1: an atlas of CCD images of 41 distant clusters. *ApJS*, 94: 583–614, October 1994. doi: 10.1086/192083.

W. Holland, M. MacIntosh, A. Fairley, D. Kelly, D. Montgomery, D. Gostick, E. Atad-Ettedgui, M. Ellis, I. Robson, M. Hollister, A. Woodcraft, P. Ade, I. Walker, K. Irwin, G. Hilton, W. Duncan, C. Reintsema, A. Walton, W. Parkes, C. Dunare, M. Fich, J. Kycia, M. Halpern, D. Scott, A. Gibb, J. Molnar, E. Chapin, D. Bintley, S. Craig, T. Chylek, T. Jenness, F. Economou, and G. Davis. SCUBA-2: a 10,000-pixel submillimeter camera for the James Clerk Maxwell Telescope. In *Society of Photo-Optical Instrumentation Engineers (SPIE) Conference Series*, volume 6275 of *Presented at the Society of Photo-Optical Instrumentation Engineers (SPIE) Conference*, July 2006. doi: 10.1117/12.671186.

W.S. Holland, W. Duncan, B.D. Kelly, K.D. Irwin, A.J. Walton, P.A.R. Ade, and E.I. Robson. Scuba-2: a new generation submillimeter imager for the james clerk maxwell telescope. *SPIE*, 4855:1, 2003. Millimeter and Submillimeter Detectors for Astronomy.

W.S. Holland et al. Scuba: A common-user submillimetre camera operating on the james clerk maxwell telescope. *MNRAS*, 303:659, 1999. arXiv:astro-ph/9809122v1.

W.S. Holland et al. Scuba-2: a 10,000 pixel submillimeter camera for the james clerk maxwell telescope. *SPIE*, 6275:45, 2006.

A.M. Hopkins, A.J. Connolly, D.B. Haarsma, and L. E. Cram. Toward a Resolution of the Discrepancy between Different Estimators of Star Formation Rate. *AJ*, 122:288, 2001.

K. D. Irwin and G. C. Hilton. *Transition-Edge Sensors*. Topics Appl. Phys. 99, 63-149. Springer-Verlag Berlin Heidelberg, 2005. Chapter in Cryogenic Particle Detection, C. Enss (Ed.).

D. Ishihara, T. Onaka, H. Kataza, A. Salama, C. Alfageme, A. Cassatella, N. Cox, P. García-Lario, C. Stephenson, M. Cohen, N. Fujishiro, H. Fujiwara, S. Hasegawa, Y. Ita, W. Kim, H. Matsuhara, H. Murakami, T. G. Müller, T. Nakagawa, Y. Ohyama, S. Oyabu, J. Pyo, I. Sakon, H. Shibai, S. Takita, T. Tanabé, K. Uemizu, M. Ueno, F. Usui, T. Wada, H. Watarai, I. Yamamura, and C. Yamauchi. The AKARI/IRC mid-infrared all-sky survey. *A&A*, 514:1, 2010.

T.H. Jarrett, T. Chester, R. Cutri, S.E. Schneider, and J.P. Huchra. The 2MASS Large Galaxy Atlas. *AJ*, 125:525, 2003.

T. Jenness, D. Berry, E. Chapin, F. Economou, A. Gibb, and D. Scott. SCUBA-2 Data Processing. *ArXiv e-prints*, November 2010a.

T. Jenness, D. Berry, E. Chapin, F. Economou, A. Gibb, and D. Scott. Scuba-2 data processing. *arXiv:1011.5876, ADASS 2010*, November 2010b.

R. Kackley, D. Scott, E. Chapin, and P. Friberg. JCMT Telescope Control System upgrades for SCUBA-2. *SPIE*, 7740, 2010. doi: 10.1117/12.857397.

J. L. Karr and P. G. Martin. Triggered star formation in the w5 h ii region. *The Astrophysical Journal*, 595(2):900, 2003. URL `http://stacks.iop.org/0004-637X/595/i=2/a=900`.

J.L. Karr and P.G. Martin. Triggered Star Formation in the W5 H II Region. *ApJ*, 595:900, 2003.

T. Kodama, M. Tanaka, T. Tamura, H. Yahagi, M. Nagashima, I. Tanaka, N. Arimoto, T. Futamase, M. Iye, Y. Karasawa, N. Kashikawa, W. Kawasaki, T. Kitayama, H. Matsuhara, F. Nakata, T. Ohashi, K. Ohta, T. Okamoto, S. Okamura, K. Shimasaku, Y. Suto, N. Tamura, K. Umetsu, and T. Yamada. Panoramic Views of Cluster-Scale Assemblies Explored by Subaru Wide-Field Imaging. *PASJ*, 57:309–323, April 2005.

X.P. Koenig, L.E. Allen, R.A. Gutermuth, J.L. Hora, C.M. Brunt, and J. Muzerolle. Clustered and Triggered Star Formation in W5: Ob-

servations with Spitzer. *ApJ*, 688:1142–1158, December 2008. doi: 10.1086/592322.

T. MacKenzie, F. G. Braglia, A. G. Gibb, D. Scott, T. Jenness, S. Serjeant, M. Thompson, D. Berry, C. M. Brunt, E. Chapin, A. Chrysostomou, D. Clements, K. Coppin, F. Economou, A. Evans, P. Friberg, J. Greaves, T. Hill, W. Holland, R. J. Ivison, J. H. Knapen, N. Jackson, G. Joncas, L. Morgan, A. Mortier, C. Pearson, M. Pestalozzi, A. Pope, J. Richer, J. S. Urquhart, M. Vaccari, B. Weferling, G. White, and M. Zhu. A pilot study for the SCUBA-2 'All-Sky' Survey. *MNRAS*, 415:1950–1960, August 2011. doi: 10.1111/j.1365-2966.2011.18840.x.

S.T. Megeath, L.K. Townsley, M.S. Oey, and A. R. Tieftrunk. *Low and High Mass Star Formation in the W3, W4, and W5 Regions*, pages 264–+. December 2008.

S. M. Moran, R. S. Ellis, T. Treu, G. P. Smith, R. M. Rich, and I. Smail. A Wide-Field Survey of Two z ˜ 0.5 Galaxy Clusters: Identifying the Physical Processes Responsible for the Observed Transformation of Spirals into S0s. *ApJ*, 671:1503–1522, December 2007. doi: 10.1086/522303.

L. K. Morgan, M. A. Thompson, J. S. Urquhart, and G. J. White. A SCUBA survey of bright-rimmed clouds. *Astronomy and Astrophysics*, 477:557–571, January 2008a. doi: 10.1051/0004-6361:20078104.

L.K. Morgan, M.A. Thompson, J.S. Urquhart, and G.J. White. A SCUBA survey of bright-rimmed clouds. *A&A*, 477:557, 2008b.

M. Negrello, R. Hopwood, G. De Zotti, A. Cooray, A. Verma, J. Bock, D. T. Frayer, M. A. Gurwell, A. Omont, R. Neri, H. Dannerbauer, L. L. Leeuw, E. Barton, J. Cooke, S. Kim, E. da Cunha, G. Rodighiero, P. Cox, D. G. Bonfield, M. J. Jarvis, S. Serjeant, R. J. Ivison, S. Dye, I. Aretxaga, D. H. Hughes, E. Ibar, F. Bertoldi, I. Valtchanov, S. Eales, L. Dunne, S. P. Driver, R. Auld, S. Buttiglione, A. Cava, C. A. Grady, D. L. Clements, A. Dariush, J. Fritz, D. Hill, J. B. Hornbeck, L. Kelvin, G. Lagache, M. Lopez-Caniego, J. Gonzalez-Nuevo, S. Maddox, E. Pascale, M. Pohlen, E. E. Rigby, A. Robotham, C. Simpson, D. J. B. Smith, P. Temi, M. A. Thompson, B. E. Woodgate, D. G. York, J. E. Aguirre, A. Beelen, A. Blain, A. J. Baker, M. Birkinshaw, R. Blundell, C. M. Bradford, D. Burgarella, L. Danese, J. S. Dunlop, S. Fleuren, J. Glenn, A. I. Harris, J. Kamenetzky, R. E. Lupu, R. J. Maddalena, B. F. Madore, P. R. Maloney, H. Matsuhara, M. J. Michaowski, E. J. Murphy, B. J. Naylor,

H. Nguyen, C. Popescu, S. Rawlings, D. Rigopoulou, D. Scott, K. S. Scott, M. Seibert, I. Smail, R. J. Tuffs, J. D. Vieira, P. P. van der Werf, and J. Zmuidzinas. The Detection of a Population of Submillimeter-Bright, Strongly Lensed Galaxies. *Science*, 330:800, 2010a.

M. Negrello et al. The Detection of a Population of Submillimeter-Bright, Strongly Lensed Galaxies. *Science*, 330:800–, November 2010b. doi: 10.1126/science.1193420.

T. Niwa, Y. Itoh, Y. Oasa, K. Sunada, K. Sugitani, and T. Mukai. Millimeter-wave survey of molecular clouds around the W5-East triggered star-forming region. *A&A*, 500:1119, 2009.

P. Prugniel and P. Heraudeau. Total magnitude, radius, colour indices, colour gradients and photometric type of galaxies. *A&AS*, 128:299, 1998.

E. D. Reese, J. J. Mohr, J. E. Carlstrom, M. Joy, L. Grego, G. P. Holder, W. L. Holzapfel, J. P. Hughes, S. K. Patel, and M. Donahue. Sunyaev-Zeldovich Effect-derived Distances to the High-Redshift Clusters MS 0451.6-0305 and CL 0016+16. *ApJ*, 533:38–49, April 2000. doi: 10.1086/308662.

I. Smail, R. J. Ivison, and A. W. Blain. A Deep Sub-millimeter Survey of Lensing Clusters: A New Window on Galaxy Formation and Evolution. *ApJ*, 490:L5, November 1997. doi: 10.1086/311017.

M. A. Thompson, S. Serjeant, T. Jenness, D. Scott, M. Ashdown, C. Brunt, and H. Butner. The scuba-2 all-sky survey. *arXiv:0704.3202v2*, 2007.

D. Ward-Thompson, J. M. Kirk, P. André, P. Saraceno, P. Didelon, V. Könyves, N. Schneider, A. Abergel, J.-P. Baluteau, J.-P. Bernard, S. Bontemps, L. Cambrésy, P. Cox, J. di Francesco, A. M. di Giorgio, M. Griffin, P. Hargrave, M. Huang, J. Z. Li, P. Martin, A. Men'shchikov, V. Minier, S. Molinari, F. Motte, G. Olofsson, S. Pezzuto, D. Russeil, M. Sauvage, B. Sibthorpe, L. Spinoglio, L. Testi, G. White, C. Wilson, A. Woodcraft, and A. Zavagno. A Herschel study of the properties of starless cores in the Polaris Flare dark cloud region using PACS and SPIRE. *A&A*, 518:L92, July 2010.

J. L. Wardlow, I. Smail, G. W. Wilson, M. S. Yun, K. E. K. Coppin, R. Cybulski, J. E. Geach, R. J. Ivison, I. Aretxaga, J. E. Austermann, A. C. Edge, G. G. Fazio, J. Huang, D. H. Hughes, T. Kodama, Y. Kang, S. Kim, P. D. Mauskopf, T. A. Perera, and K. S. Scott. An AzTEC 1.1-mm survey

for ULIRGs in the field of the Galaxy Cluster MS0451.6-0305. *MNRAS*, 401:2299–2317, February 2010. doi: 10.1111/j.1365-2966.2009.15847.x.

D. V. Wiebe, P. A. R. Ade, J. J. Bock, E. L. Chapin, M. J. Devlin, S. Dicker, M. Griffin, J. O. Gundersen, M. Halpern, P. C. Hargrave, D. H. Hughes, J. Klein, G. Marsden, P. G. Martin, P. Mauskopf, C. B. Netterfield, L. Olmi, E. Pascale, G. Patanchon, M. Rex, D. Scott, C. Semisch, N. Thomas, M. D. P. Truch, C. Tucker, G. S. Tucker, and M. P. Viero. BLAST Observations of Resolved Galaxies: Temperature Profiles and the Effect of Active Galactic Nuclei on FIR to Submillimeter Emission. *ApJ*, 707:1809, 2009.

I. Yamamura, S. Makiuti, N. Ikeda, Y. Fukuda, S. Oyabu, T. Koga, and G.J. White. AKARI/FIS All-Sky Survey Point Source Catalogues (ISAS/JAXA, 2010). *VizieR Online Data Catalog*, 2298:0–+, 2010.

Appendix A

ALMA Proposal: disentangling a lensed group of galaxies at z=2.9

Introduction Gravitational lensing has been a huge boon for enabling sub-mm studies. The first results from SCUBA [Smail et al., 1997] used "nature's telescope" to increase the detection rate and effectively beat the confusion limit for single dish studies. Now *Herschel* has found that lensing is significant for some of the brightest sub-mm sources, with surveys such as H-ATLAS and HerMES turning up a population of objects which are boosted enough that they can be studied in great detail in follow-up observations (e.g. [Negrello et al., 2010b]). However, the limited beam-size of *Herschel*, and of non-interferometric ground-based instruments, means that the effects of source blending are a cause of uncertainty in interpreting the results, made even worse in practice, since submm-bright sources are known to be typically merging or interacting systems, where disentangling the contribution to the combined spectral energy distribution (SED) is more complicated still. And even worse – strong lensing in such extended systems is *not* achromatic, since different parts of the interacting system can be lensed by different amounts in different wavebands. Thus the existence of strong lensing can be a double-edged sword, boosting the brightness of some sources, but making the detailed interpretation of their SEDs problematic.

For the simpler case of cluster lensing, ALMA has the resolution and sensitivity required in order to break up the submm emission so that it can be directly compared with the $\sim 1''$ imaging available in the radio and in the near-IR through to optical, so that the multi-wavelength lensed images can be disentangled.

We propose to observe the field of MS 0451.6−0305, a massive galaxy cluster at a redshift of 0.54 which is lensing several background sources and has been imaged at many different wavelengths: radio [Reese et al., 2000, Berciano Alba et al., 2010]; mm/submm [Borys et al., 2004, Wardlow et al.,

2010]; far-IR (part of HerMES); mid-IR [Geach et al., 2006]; near-IR [Borys et al., 2004, Wardlow et al., 2010]; optical [Gioia and Luppino, 1994, Moran et al., 2007, Kodama et al., 2005]; and X-ray [Donahue et al., 2003]. In the optical the lensed objects include an extended arc as well as two extremely red objects (EROs) and a Lyman-break galaxy (LBG) [Borys et al., 2004]. The two EROs and the LBG are at a redshift of approximately 2.9 and although distinct, are so close in separation that they must constitude an interacting system [Borys et al., 2004]. In the radio and mid-IR it is clear that several other sources are being lensed – presumably components within the same galaxy group. The steep number counts in the submm make lensing much more striking in this waveband – at 850 μm SCUBA showed a "giant submm arc", stretching about 1 arcminute, consistent with the blending of several galaxy images which lie near the critical line in the lens model. With ALMA, we will be able to resolve this submm emission and attribute the individual compenents to the objects already known to make up the lensed group, as well as possibly identifying new objects or components. ALMA will enable a detailed case study to be made of this unique $z = 2.9$ system, with valuable lessons to be learned for interpreting multi-wavelength data from other strongly lensed sources.

Previous studies of this lensing system The cluster was recently observed with SCUBA-2 [Holland et al., 2006] during commissioning, as part of "Guaranteed Time" for the instrument team. Since the submm arc had already been observed at 850 μm using SCUBA, the motivation for the new observations were: (1) to confirm the bright lensed structure with SCUBA-2, without the complications introduced by SCUBA's requirement to chop; and (2) to detect the lensed structure at 450 μm, with resolution better by about a factor of two. The images were taken in weather which was good enough to obtain 450 μm detections, with the hope of breaking up the arc into sources. The size of the new map (made with one sub-array at each wavelength) is about an order of magnitude larger in area than the original SCUBA image, but still not large enough to encompass the entire cluster.

At 850 μm, the submm arc is easily detected by SCUBA-2. It is elongated roughly north-south, and at the southern end, curves to the west, just as in the original SCUBA image. The higher-resolution 450-μm data trace a largely similar structure which also closely mimics the shape of the optical lensed features (see Fig. A). After applying a PSF-matched filter, the 450 μm emission breaks up into two main sources. At 850 μm the flux densities for these two components are approximately 7 mJy and 15 mJy, giving S_{850}/S_{450} flux density ratios of around 0.5 and 1.0, consistent with the high redshift

of the lensed sources (although with large uncertainty). The morphology of the lens at 450 μm appears somewhat different from what might have been expected based on existing observations. So the lensing story continues to be complicated and higher resolution submm imaging is what is really needed.

Previous studies of this cluster core have shown strong lensing and multiple images, but different lensed sources are identified in different wavebands. For comparison purposes, sources identified in earlier are overplotted onto the new 450 μm and 850 μm data – Fig. A compares lensed images identified in the optical, near-IR and radio. Without the higher resolution imaging of ALMA, it is impossible to determine which of these are contributing to the giant submm arc.

Fig. A shows a comparison between the new SCUBA-2 450 μm contours with: the VLA 1.4 GHz map from Berciano Alba et al. [2010] (left panel); and the 24 μm *Spitzer* image (right panel). The correspondence looks extremely promising, although the SCUBA-2 data, even at 450 μm has failed to break up the submm emission.

ALMA technical justification and simulations

We propose to observe the submm lensed arc using ALMA Band 7 at 343 GHz, corresponding closely to the peak wavelength of the 850 μm filter of SCUBA-2, while also avoiding nearby atmospheric absorption lines. In the original SCUBA image, it was found that the submm arc intensity was 10 mJy beam^{-1} over several beam areas, with an equivalent of $\sum S > 30$ mJy if we consider it as a blending of point sources. Let us therefore assume that we have a set of sources (by which we mean objects in the image plane) of flux density each of ~ 5 mJy at 850 μm. Achieving an rms of 0.3 mJy would give us high SNR for these objects and allow us room for error in our estimated flux densities, as well as the possibility of detecting new or extended components of the lens. Covering the arc area with 18 pointings, with 3.9 minutes per pointing to achieve the desired sensitivity, results in a 1.17 hour on-source integration time and an estimated 1.42 hours total estimated time (including Calibration).

To simulate the proposed ALMA observation in more detail, including the possibility that lensed images are partially resolved, we used a model consisting of 1.6″ FWHM images (this is approximately 12 kpc diameter at $z = 2.9$), placed at the locations found by Berciano Alba et al. [2010]. All these images have roughly the same flux density in the radio, and so we use the same submm brightness, except for "RJ" (see Fig. A), which is thought to be a radio jet, to which we attributed half of the flux density of the others. For the purpose of our science goals, we wish to resolve the giant submm

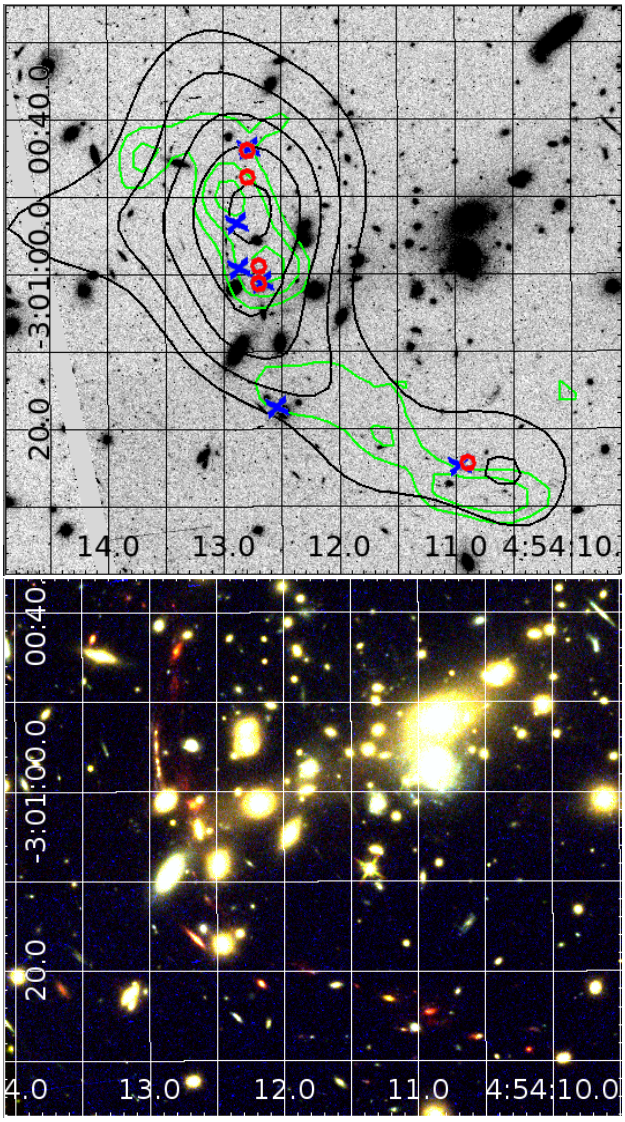

Figure A.1: *Top*: *HST* image of MS 0451−03 with SCUBA-2 850 μm contours (black), SCUBA-2 450 μm contours (green), two multiply imaged EROs (red cicles), an optical arc comprising of a multiply imaged LBG (more obvious in right hand figure), and radio sources detected by [Berciano Alba et al., 2010] (blue crosses). *Bottom*: new *HST* WFC3 colour-composite, clearly showing the main optical arc (roughly vertical, at about RA = 13.0) offset from the abundance of red images along the Einstein ring. Disentangling the sources contributing to the submm emission will require ALMA's sensitivity and angular resolution.

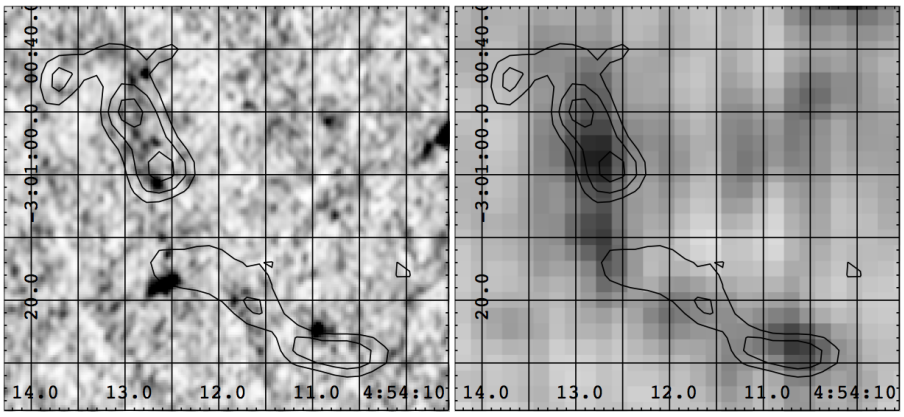

Figure A.2: *Left*: 1.4 GHz VLA image with SCUBA-2 450 μm contours overlaid. *Right*: 24 μm MIPS image data with SCUBA-2 450 μm contours overlaid. The 450 μm resolution is certainly better than at 850 μm, and the correspondence with the mid-IR and radio is obvious – but which of these objects are contributing to the submm arc?

arc into separate galaxy counterparts, and thus the 1.4 arcsec resolution of the compact configuration is sufficient for our purposes and we are able to cover the lens area using 18 individual pointings. Fig. 3 shows the result of a noiseless simulation using SIMDATA.

Fig. A shows the reconstructed source plane of our toy model. The fidelity of the current VLA data (from which our toy model is derived) and the lensing model of the cluster is clearly shown in the source reconstruction, as five of ALMA "sources" are shown to be multiple images of two objects. We plan to carry out this same kind of source-plane reconstruction at all available wavebands, to understand the effects of differential amplification on the $z = 2.9$ galaxy group.

Publication and media promotion possibilities

Gravitational lensing has always been an attention grabber for the public media ever since it was first observed by Arthur Eddington in 1919, and beautiful cluster lenses have become familiar in the last couple of decades. Strong lensing in the submm can be visually striking, and in the case of MS 0451−03 actually dominates the image as a whole. Combining ALMA observations with the current *HST* image, showing the optical arc and multiply lensed EROs and LBG, would be an immediate eye-catcher and demonstrate to the public that ALMA is indeed a success.

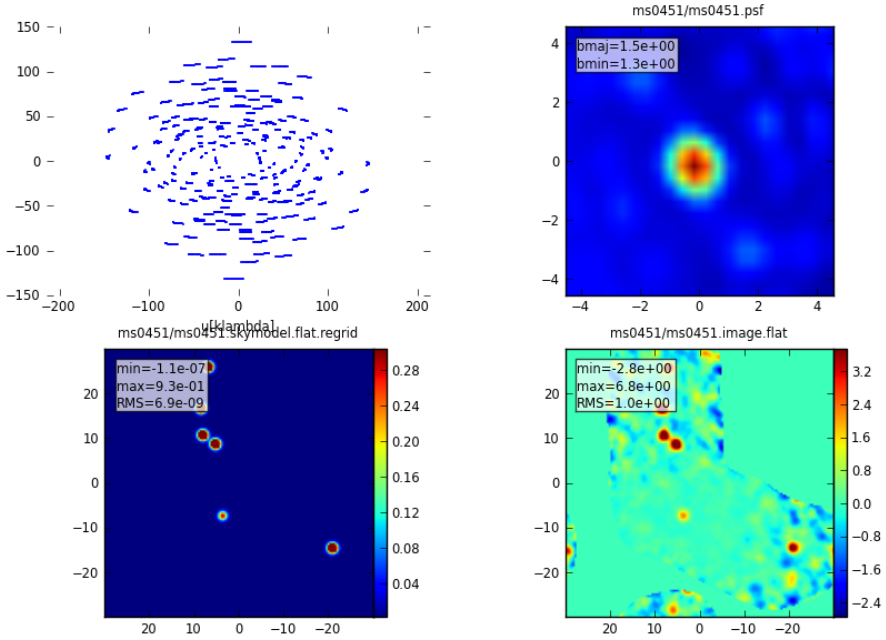

Figure A.3: Noiseless simulation of the model based upon radio sources from Berciano Alba et al. [2010]. The simulation was carried out using the compact array configuration at 350 GHz (ALMA band 7). Apparent structure in the bottom right panel is due to incomplete u, v sampling, but will not affect our ability to discriminate sources.

Within the scientific community, using ALMA to disentangle the lensing story behind one of these much-talked-about submm lenses would demonstrate that ALMA is the instrument of choice for such systems. Included in the publication would be the new SCUBA-2 observations, demonstrating the complementary capabilities of these two instruments. Our team includes several members of the SCUBA-2 instrument group, as well as experts on submm galaxies, interferometry, multi-wavelength modelling, and lensing – thus our publication turn-around time should be short.

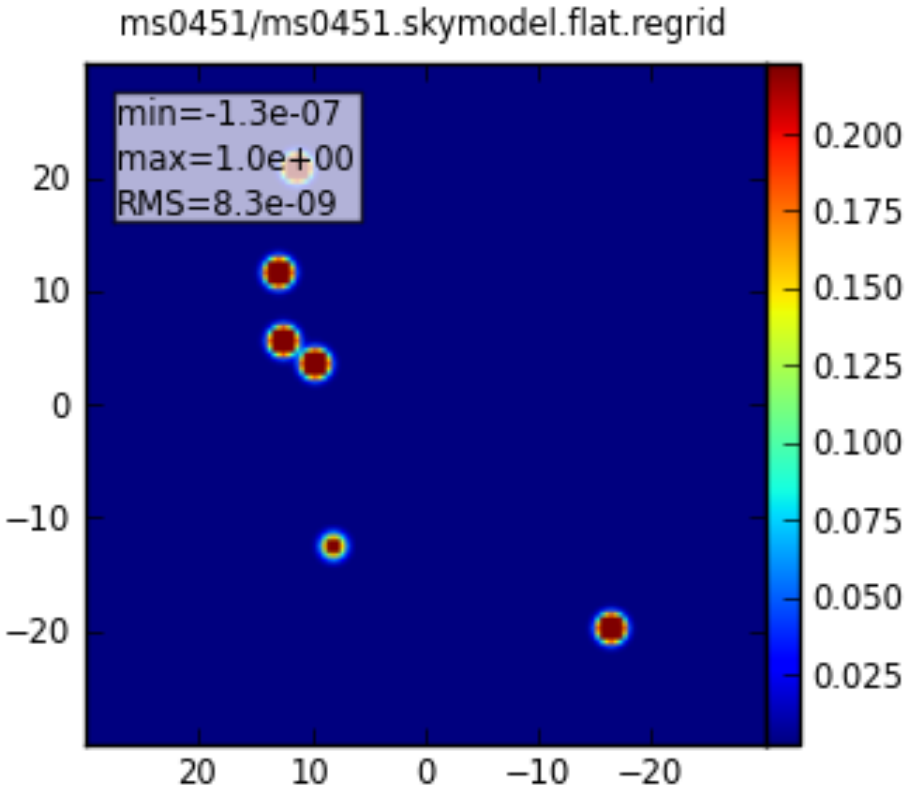

Figure A.4: *Left*: toy model for what may be detected by ALMA. *Right*: reconstruction of the source plane based on the existing lensing model for the cluster. The three images circled in green correspond to the (resolved) green circled object in the source plane, and similarly for the two images circled in red in the left panel. Combining lensing reconstructions at different wavebands will allow us to build up a picture of the spatially-resolved SED of the $z = 2.9$ galaxy group.